Chemical Geology 476 (2018) 441–455

Contents lists available at ScienceDirect

Chemical Geology

journal homepage: www.elsevier.com/locate/chemgeo

Dual-phase mass balance modeling of small mineral particle losses from sedimentary rock-derived soils

Carleton R. Bern[a,b,*], Tiffany Yesavage[b]

[a] Colorado Water Science Center, U.S. Geological Survey, Denver Federal Center, Denver, CO 80225, USA
[b] Crustal Geophysics and Geochemistry Science Center, U.S. Geological Survey, Denver Federal Center, Denver, CO 80225, USA

ARTICLE INFO

Keywords:
Colloids
Dual-phase mass balance model
Pedogenesis
Susquehanna/Shale Hills Critical Zone Observatory
Zirconium mobility

ABSTRACT

Losses of small mineral particles can be a significant physical process that affects the elemental composition of soils derived from sedimentary rocks. Shales, in particular, contain abundant clay-sized minerals that can be mobilized by simple disaggregation, and solutional weathering is limited because the parent rock is composed primarily of recalcitrant minerals previously subjected to continental weathering. Here, the dual-phase mass balance model is employed to quantify losses of small mineral particles as water dispersible colloids (WDCs) from three previously studied soil profiles along a hill slope at the Susquehanna Shale Hills Critical Zone Observatory (SSHO). WDCs were isolated from soil in the laboratory to determine their mineralogical and elemental compositions. Clay minerals dominated WDCs, including illite, vermiculite, and chlorite inherited from the parent shale, along with neoformed kaolinite. Quartz present in bulk soil was generally excluded from WDCs. Elements of low solubility and/or bound in recalcitrant forms, like Rb in illite, were employed in tracer ratios in the dual-phase model. Aluminum, Ga, and Rb were enriched in WDCs, and Zr and Hf were partially excluded. Six different combinations of elements into tracer ratios (Al/Zr, Ga/Zr, Rb/Zr, Al/Hf, Ga/Hf, Rb/Hf) each yielded similar model results. Mass losses of WDCs were large, ranging from $-68 \pm 7\%$ to $-15 \pm 5\%$ relative to soil parent material in different parts of the profiles. Mass losses via solution were smaller, ranging from $-7 \pm 2\%$ to a gain of $6 \pm 1\%$ in part of one profile. Losses of WDCs account for > 90% of total mass loss, surpassing chemical dissolution, and therefore dominate the weathering portion of denudation at SSHO. Zirconium concentrations were 97–158 ppm in the generally ≤ 1 μm WDCs, suggesting colloidal, Zr-bearing phases. Model-quantified losses of Zr via WDCs were large, with a median loss of 41% relative to parent material. Such losses indicate systematic underestimates of weathering by traditional mass balance that uses Zr as an index element. Losses of Ca, Mg, and K via WDCs exceeded losses via solution, countering assumptions of base cation losses primarily via mineral dissolution. The results illustrate a geochemical fingerprint of physical weathering and the ability of the dual-phase model to quantify that weathering process.

1. Introduction

Weathering is a collection of both chemical and physical processes that exert tremendous control over the nature of soils in Earth's Critical Zone. Chemical weathering includes processes like hydrolysis, dissolution, oxidation, and complexation, which commonly place elements in solution and thus allow transport and loss via water. Physical weathering breaks down rock into smaller particles, increasing surface area for chemical reactions and increasing transportability. Erosion is another physical process that transports material disaggregated by weathering from one location to another. Generally, whether erosion occurs by soil creep, landslide, or biogenic processes like tree throw, it is considered to act upon soil as a bulk material. Thus, the material-removal portion of the erosion process is often assumed to have little geochemical influence on soils compared to chemical weathering.

Within soil, however, smaller particles can be mobile relative to the surrounding matrix (Jenny and Smith, 1935). Where these particles have a distinct geochemical composition, there is potential for their mobility to alter elemental composition of horizons within the soil profile, as well as elemental fluxes out of soil and therefore the composition of the residual matrix (Barshad, 1955; Sudom and St. Arnaud, 1971). Such small mineral particles may be produced chemically as precipitated secondary phases, and also physically by disaggregation and fracturing of inherited phases. Production is different from mobilization and transport, and mobilization can be triggered by both chemical dispersion and physical shear stress (El-Farhan et al., 2000;

* Corresponding author at: Colorado Water Science Center, U.S. Geological Survey, Denver Federal Center, Denver, CO 80225, USA.
E-mail address: cbern@usgs.gov (C.R. Bern).

https://doi.org/10.1016/j.chemgeo.2017.11.040
Received 13 July 2017; Received in revised form 10 October 2017; Accepted 27 November 2017
Available online 06 December 2017
0009-2541/ Published by Elsevier B.V.

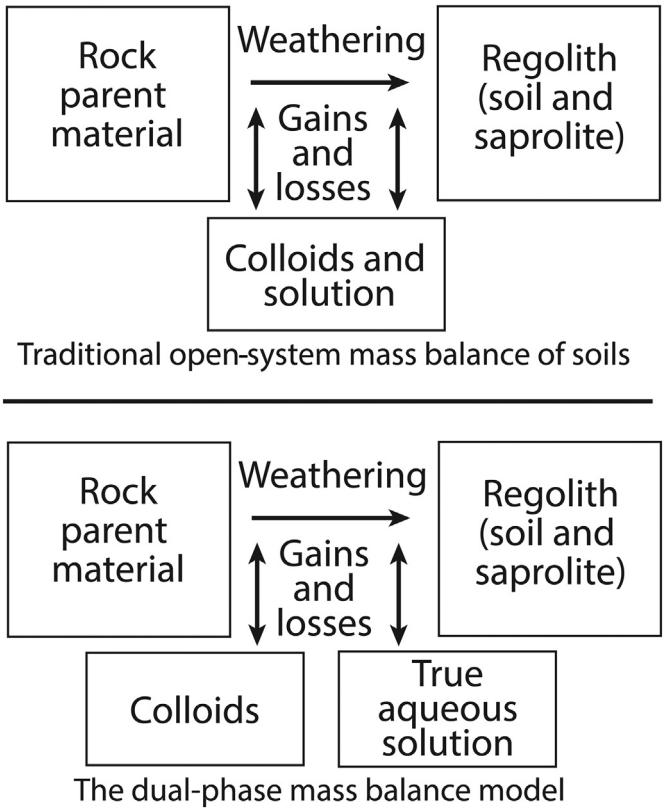

Fig. 1. Cartoon illustrating how lumped mass transfers from the traditional open-system mass balance (top panel) are divided into colloidal and dissolved components by the dual-phase mass balance model (bottom panel).

Lægdsmand et al., 1999). Once mobilized, small mineral particles can behave as colloids, which are the generally ≤ 1-μm particles that tend to remain suspended in solution and thus water facilitates their mobility.

The dual-phase mass balance model has been formulated specifically to quantify the geochemical effects of colloid mobility and distinguish those from solutional processes (Fig. 1; Bern and Chadwick, 2010; Bern et al., 2011; Bern et al., 2015). For the dual-phase model, selected elements are assumed to be insoluble, and mobility of those elements occurs solely as colloids moving relative to the soil matrix. Preferential inclusion and exclusion of these selected elements in the colloids allow their concentrations to be used in ratio form to trace gains or losses of colloidal material. A secondary benefit to the model is that it eliminates the necessity of assuming immobility for Zr or another index element (e.g., Brantley and White, 2009; Brimhall et al., 1991; Merrill, 1897) and instead quantifies Zr mobility. To date, the dual-phase model has only been applied to a single site, a gently sloping, granitic *catena* developed under a semiarid climate in Southern Africa (Bern et al., 2015). There, mass losses due to colloid movement were relatively small (−14%), and downslope soil horizons had gained significant (56%) colloid mass. To expand understanding of the importance of colloid movement in soils, and the means by which it may be traced, the present study applies the dual-phase model to a quite different setting, soils on relatively steeper slopes, derived from shale, and formed under a temperate climate.

Mobility of colloids has already been identified as an important process at the Susquehanna/Shale Hills Critical Zone Observatory (SSHO) through a range of investigations employing elemental, isotopic, and mineral mass balance approaches (Jin et al., 2010; Ma et al., 2010; Ma et al., 2011b; Ma et al., 2015; Noireaux et al., 2014; Sullivan et al., 2016b; Yesavage et al., 2012). Micron-sized mineral particles appear to be transported relative to the soil matrix, primarily by subsurface lateral flow through macropores and along interfaces between soil horizons, and between soil and bedrock (Graham and Lin, 2011; Lin, 2006). Considerable quantities of particulate losses are indicated by substantial mass losses of elements less soluble under prevailing weathering conditions (Jin et al., 2010; Ma et al., 2010; Ma et al., 2011a) and isotopic mass balances for Fe, Mg and B that are best explained by losses of micron-sized particles with particular compositions (Ma et al., 2011a; Noireaux et al., 2014; Yesavage et al., 2012). However, the magnitudes of colloidal losses, relative to dissolved losses, have not been quantified because that is beyond the ability of the traditional mass balance model. Nevertheless, the prior knowledge of the great importance of colloid losses at SSHO make it an ideal setting to explicitly quantify dissolved and colloidal losses using the dual-phase model.

The goals of the present study are therefore twofold. The first is to illustrate how the dual-phase model may be applied to sedimentary rock-derived soils. The Ti/Zr tracer ratio used in the previous model application is unsuitable at SSHO and multiple elemental tracers are considered and used in the model. The second goal is to quantify elemental losses in dissolved and colloidal forms at SSHO and demonstrate the insights gained by doing so.

2. Materials and methods

2.1. Setting and samples

The SSHO is an 80,000-m^2, V-shaped catchment that contains an ephemeral stream. It is located in the Appalachian Mountains in central Pennsylvania, USA, and has a mean annual temperature (MAT) of 10 °C and mean annual precipitation (MAP) of 107 cm (Jin et al., 2010). The bedrock from which soils have formed is the Silurian-age Rose Hill Formation, a shale with a few, thin, interbedded sandstones (Lynch, 1976). Presence of feldspars in soils (1.2–6.6 wt%), and sparse to absent feldspar presence (≤ 0.5 wt%) in the shale (Jin et al., 2010), suggest a minor, feldspar-bearing aeolian component to the soils. SSHO is located outside the boundary of Pleistocene continental glaciation, and thicker Pleistocene aeolian deposits blanket landscapes to the east and west (Markewich et al., 2015). Soils in the watershed include the predominant Weikert soil series (Lithic Dystrudepts), but convergent areas contain the Berks (Typic Dystrudepts), and soils approximating the Blairton (Aquic Hapludults) and Rushtown (Typic Dystrochrepts) series, and along the valley floor soils approximating the Ernest (Aquic Fragidults) series are present (Soil Survey Division Staff, 1993; Lin, 2006). Hillslopes at SSHO are generally convex near ridgetops and planar along middle slope sections, and the southern slope is steeper (~20°) than the northern slope (~15°; West et al., 2013). Soil is thin (~30 cm) at ridge crests but deposits up to 300 cm thick occur along the valley floor (Lin et al., 2006). Vegetation is dominated by trees including maple (*Acer* spp.), oak (*Quercus* spp.) and hickory (*Carya* spp.), with eastern hemlock (*Tsuga canadensis*) on the valley floor.

For this study, colloids were extracted from splits of selected depth profile samples collected at locations coincident with other studies that examined bulk soil geochemistry at SSHO (Jin et al., 2010; Ma et al., 2013; Ma et al., 2011a). The profiles are from a planar (nonconvergent) hillslope on the southern side of the catchment and include ridgetop (SPRT; 30-cm depth), middle slope (SPMS; 59-cm depth), and valley floor (SPVF; 67-cm depth) positions. The samples used for this study reached different maximum depths for the ridgetop (SRT; 25-cm depth), middle slope (SMS; 46-cm depth), and valley floor (SVF; 105-cm depth). In all cases, profiles were divided into 10-cm increments, and maximum depth indicates the depth of auger refusal.

2.2. Water-dispersible colloid extraction and analysis

The dual-phase model requires a representation of the elemental composition of colloidal material that is mobile relative to bulk soil.

The term water dispersible colloids (WDCs) is used here to refer to the material extracted from soil in the laboratory. Previous studies have found compositional similarities between WDCs extracted in the laboratory and colloids mobile in soil- and stream waters (Bern et al., 2015; Kaplan et al., 1997; Mills et al., 2017). The extraction method described here is a modification of that from Bern et al. (2015).

To extract WDCs, 23 g of air dried soil, sieved to < 2 mm and 207 g of ultrapure water (18.2 MΩ/cm) were placed in a 250-mL plastic bottle (1:10 soil:solution). Bottles were placed on a side-to-side table shaker for 10 min of shaking at approximately 100 rpm. The bottles were centrifuged for 4 min at 2000 rpm in a RC5C Sorvall® Instruments centrifuge with a swinging bucket HS-4 Sorvall® rotor to settle sand- and silt-size material. After careful removal from the centrifuge, the supernatant from each bottle (~170 mL) was siphoned to a flask by vacuum. To remove low-density root material and larger mineral particles, the supernatant was then passed through a 1-μm nylon mesh (Elko Filtering Co., Miami, Florida) on a plastic frame that exposed ~108 cm^2 of mesh. The 1-μm physical limit was selected because it has been previously suggested as relevant for SSHO soils (e.g., Jin et al., 2010) and to easily filter large volumes of suspension and thus obtain substantial masses of WDCs. The mesh was pre-treated by soaking briefly in methanol to remove manufacturing residue and then pre-wetted with deionized water to aid supernatant filtering. Eight rounds of shaking, centrifugation, and siphoning were performed for each 23-g sample to maximize yield. Filtered supernatant (~1400 mL) was weighed and oven dried in polytetrafluoroethylene vessels at 90 °C to determine mass yields. Splits of select samples were taken for particle-size and mineralogical analysis.

Elemental concentrations in dried WDC materials were determined by SGS Mineral Services (Lakefield, Ontario, Canada). Powdered samples were sintered using sodium peroxide, then dissolved in nitric acid with an addition of tartaric acid. Aliquots were analyzed by inductively-coupled plasma mass-spectrometry (ICP-MS). Blind standards constituted ~10% of submissions and results were considered satisfactory if within ± 5% to ± 20% of expected values, depending upon the element and proximity to the reporting limit.

The truly dissolved component associated with the WDC suspension was separated using 3 kDa Macrosep® Advance Centrifugal Device ultrafilters (Pall Corporation; 20-mL volume). Filters were pre-cleaned as described in Bern et al. (2015). To remove larger particles prior to ultrafiltration 15 mL of the 1 μm-filtered suspension was centrifuged at 3500 rpm for 30 min in a benchtop centrifuge. The supernatant was collected, added to ultrafilters and centrifuged at 3500 rpm for 40 min. Solution passing through the filter was acidified to pH < 2 with trace-metal grade nitric acid and analyzed by ICP-MS at Mineral Resources Program laboratories of the USGS in Denver, Colorado. Concentrations in blanks were below reporting limits for elements reported here, and blind standards were within ± 20% of expected values.

Clay mineral identification of WDCs from the < 1 μm-filtered material was accomplished by scanning oriented mounts (untreated dry, glycolated, 400 °C, 550 °C) and random powder mounts on a Panalytical X'pert Pro diffractometer (Poppe et al., 2001). Particle-size distributions were measured on splits of dispersed WDCs that had not been subjected to additional segregation by settling. Dissolved $Na_6P_6O_{18}$ was added as a dispersant to the splits to achieve a concentration of 0.25 wt%. Splits were further dispersed in a sonicating bath for 6 min, allowed to equilibrate overnight, and then sonicated for another 6 min. Particle size was determined by laser diffraction on a Mastersizer 2000 coupled to Hydro 2000G and using active sonication (Malvern Instruments Inc., Westborough, Massachusetts). A particle refractive index of 1.53 and particle absorption index of 0.01 or 0.001 were used. Residuals for particle size models of diffraction data were < 4 and may have been negatively influenced by the non-spherical nature of the colloids. WDC composition and particle-size data are available from http://criticalzone.org/shale-hills/.

In an attempt to further segregate extracted WDC material into larger and smaller size fractions, some duplicate 1 μm-filtered supernatants were made and subjected to benchtop settling in two steps. The supernatants were placed in 2-L glass beakers. In the first step, the suspension was 13.5 cm in height and material that settled to the base of the beaker was collected after 21 h at room temperature. Then, the remaining suspension was vigorously stirred. In the second step, the suspension was 12.3 cm in height and material that had settled to the base of the beaker after 96 h at room temperature was separated from the remaining suspension. Where mass yields were sufficient, splits were submitted for elemental analysis. Splits were also examined using the scanning transmission electron microscopy (STEM) detector on an FEI Quanta 450 FEG scanning electron microscope. The observation of many plate-shaped particles indicated that settling times were likely ineffective in producing consistent size fraction segregation because of slower settling for platy versus more spherical particles.

2.3. Dual-phase mass balance modeling

The dual-phase model adapts the framework and equations of a two-endmember isotope mixing model to trace the gains and losses of colloidal material in soil. Gains and losses not accounted for by colloidal material are attributed to solution processes. The model is fully derived in Bern et al. (2015); here, a shorter description of the calculations as applied at SSHO is presented.

The mass (M) of any volume of soil (kg) may be defined (Fig. 1):

$$M_s = M_p + M_c + M_d \quad (1)$$

Here the subscripts refer to soil (s), parent material (p), mass gained or lost via colloidal material (c), and mass gained or lost via solution (d). Note that M_s indicates unsieved soil, as opposed to the previous formulation that addressed sieving of soil to remove the gravel (> 2 mm) fraction (Bern et al., 2015). The mass of soil is defined:

$$M_s = V_s \rho_s \quad (2)$$

Here V_s is the volume of soil (m^3) and ρ_s is its bulk density (kg/m^3). Volume and density cancel out in certain outputs from the model that are dimensionless, such as the tau (τ) values described below. Thus, measurements of V_s and ρ_s are not strictly necessary and except as noted later, only dimensionless results are presented for SSHO. The mass of an individual element, j, in the soil component may be calculated using its concentration (C) in units of mg/kg:

$$m_{j,s} = M_s C_{j,s} \quad (3)$$

Such masses for the other three components are determined in later modeling steps and relate to each other for individual elements in the same way that overall component masses relate in Eq. (1).

A core concept of the model is that ratios of elements preferentially included, i, in colloidal material to elements preferentially excluded, e, from colloidal material are used as tracers.

$$R_{i/e} = \frac{C_i}{C_e} \quad (4)$$

In the previous application of the model, Ti was the element preferentially included and Zr was the element preferentially excluded from colloidal material. The designations i and e illustrate that other elements may be substituted as appropriate. The term preferentially excluded should not be interpreted to mean absent. Values of C_i and C_e are measured concentrations of the elements in a given component, both in mg/kg. The ratio $R_{i/e}$ can be abbreviated to R, and the ratios are designated R_s for soil, R_p for the soil parent material, and R_c for the colloidal material. The ratio in a given mass of soil reflects the masses (m) of elements i and e inherited from parent material (e.g., $m_{e,p}$) and gained or lost (positive or negative) via colloidal material (e.g., $m_{e,c}$), as well as reflecting the ratios of the parent material and colloidal components as weighted by the mass of element e:

$$R_s = \frac{m_{i,c} + m_{i,p}}{m_{e,c} + m_{e,p}} = \frac{R_c m_{e,c} + R_p m_{e,p}}{m_{e,c} + m_{e,p}} \quad (5)$$

Such a model formulation assumes that gains or losses via solution of the elements used as tracers, i and e, are negligible. Rather those elements are only gained or lost by colloidal material of the defined composition.

A parameter termed upsilon (υ) is defined as the proportion of element e gained or lost from a given mass of soil via the colloidal component:

$$\upsilon = \frac{m_{e,c}}{m_{e,c} + m_{e,p}} = \frac{m_{e,c}}{m_{e,s}} \quad (6)$$

The proportionality parameter υ can be calculated from the tracer ratios in a formulation essentially identical to that used in two-component isotopic mixing (Bern et al., 2015):

$$\upsilon = \frac{R_s - R_p}{R_c - R_p} \quad (7)$$

The mass of e gained or lost from soil via colloids is then determined:

$$m_{e,\,c} = \upsilon m_{e,\,c} \quad (8)$$

The mass of e in the parent material from which the soil was formed is then determined:

$$m_{e,p} = m_{e,s} - m_{e,c} \quad (9)$$

The total mass of parent material that gave rise to the soil (M_p), is then determined from $m_{e,p}$ and $C_{e,p}$ by rearranging Eq. (3) to solve for M_p. The total mass of colloids (M_c) can be similarly determined. The total mass of material gained or lost via solution (M_d) is then determined by rearranging Eq. (1). Overall mass change in soil due to solution processes is expressed by the ratio M_d/M_p, and overall mass change due to colloidal redistribution is expressed by the ratio M_c/M_p.

The mass of a non-tracer element, j, associated with each of the various components is then determined by using its individual concentrations in Eq. (3). Then, the mass of j gained or lost via solution is determined:

$$m_{j,d} = m_{j,s} - m_{j,p} - m_{j,c} \quad (10)$$

Traditional open-chemical-system transport functions (Brimhall et al., 1991), commonly known as τ values, combine gains and losses that occurred via both solution and colloids (Fig. 1). The dual-phase model calculates these separately, and the τ value for the dissolved component of element j is then calculated:

$$\tau_{j,d} = \frac{m_{j,d}}{m_{j,p}} \quad (11)$$

Substituting $m_{j,c}$ in the numerator yields $\tau_{j,c}$ for the colloidal component.

In addition to the assumption of negligible movement of the tracer elements in solution, other assumptions underlie the dual-phase model. It must be assumed that elemental characterization of colloidal and parent materials accurately represent those materials relative to the soil considered. This assumption is particularly uncertain relative to colloidal material, for which composition may vary by size ranges which exhibit different mobility. Colloid compositions may also change over the course of soil development. It must also be assumed that exogenous material like dust contributes negligibly to masses of tracer elements in soil. Atmospheric inputs of non-tracer elements will manifest as solution gains in model output.

As described, the dual-phase model uses concentrations of elements measured in soil, parent material, and colloidal material to determine actual gains and losses of overall mass and individual elements via colloidal material and via solution. Here, previously reported concentrations of elements in parent material and soil are used in the model (Jin et al., 2010; Ma et al., 2011a) along with element concentrations in WDCs isolated for this study. Other elements may be substituted for Ti and Zr as tracers in the model, provided the case can be made for negligible solution losses. As Ti/Zr ratios insufficiently distinguished WDCs from soil or parent material, the case is made below for using Al, Ga, and Rb concentrations in the numerator of the tracer ratio in the model. Both Zr and Hf concentrations are used in the denominator of the tracer ratio.

Justification for using the selected elements as tracers in the model is based upon examinations of similarities and differences in geochemical behavior. However, the closed nature of elemental composition datasets, in which the concentration of all possible components must sum to 100%, can generate false correlations. Thus, transforms can be useful for elucidating true correlations (Reimann et al., 2008) and a centered logratio (clr) transformation is applied here. This transformation divided each element concentration for an individual sample by the geometric mean of all the element concentrations for that sample and then took the base 10 logarithm as is illustrated here for Al.

$$clr\,(C_{Al}) = log_{10}\left(\frac{C_{Al}}{\sqrt[n]{C_1 C_2 \bullet\bullet\bullet C_n}}\right) \quad (12)$$

Pearson correlations were determined using the R software (v 3.2.3; R Core Team, 2015). Calculations using the dual-phase model are provided as Excel spreadsheets (Microsoft Corporation) in an electronic supplement to this article.

3. Results

3.1. Water-dispersible colloid characteristics

Yields from the WDC extraction method ranged 0.3–1.4 g (1–6% of sample mass) with samples from greater depth and distance downslope generally yielding more mass. Particle-size distributions of dispersed WDCs not subjected to segregation by settling showed a bimodal distribution with relatively subtle differences between samples (Fig. 2). The peak accounting for more particles is around 0.13 μm and the other peak is around 0.8 μm. Agglomeration of particles was observed during method testing using shorter equilibration times with the $Na_6P_6O_{18}$ dispersant. Therefore, although the bimodal distributions in Fig. 2 could be influenced by agglomeration, any such affect has been reduced.

The STEM images of colloids from the settling tests showed an abundance of platy clay minerals. (Fig. 3) A substantial fraction of these particles were > 1 μm across, but their platy morphology allowed them to pass through the 1 μm mesh. Denser, smaller particles accounted for a small fraction of observed particles. Some of these had angular outlines that suggest crystalline material and others were rounded, possibly indicating amorphous material. The platy nature of many particles

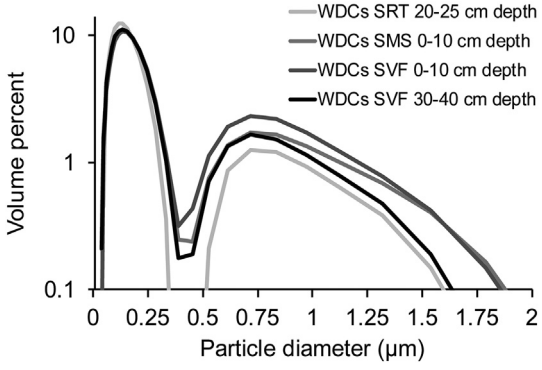

Fig. 2. Particle-size distributions of WDCs not subjected to further segregation by settling. Soils are from ridgetop (SRT), middle slope (SMS), and valley floor (SVF) profiles.

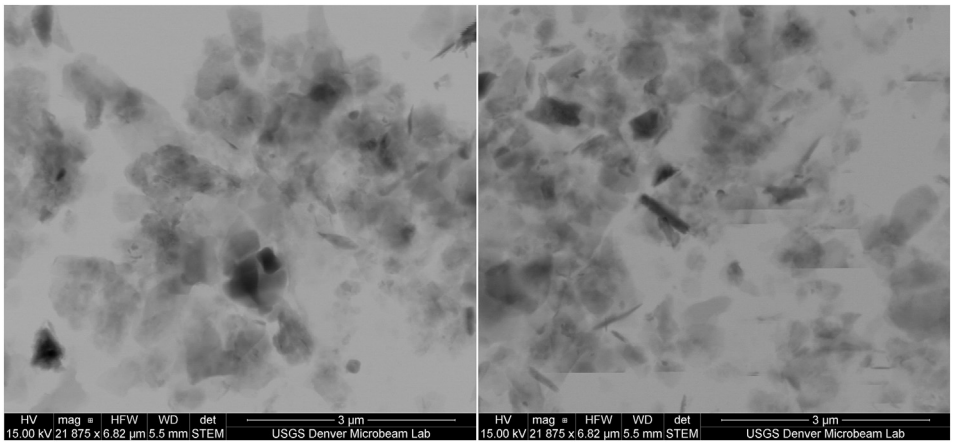

Fig. 3. Scanning transmission electron microscopy (STEM) images of extracted colloidal material from two of the settling tests. Left panel is material that settled out of suspension after 21 h; right panel is material that settled out after 96 h. Denser and thicker material appears darker in the images. Many of the particles are platelets of clay based upon broad but thin morphology. No strong differences are observed due to settling, mirroring the elemental results (Table 1).

illustrates the challenge they posed to particle-size measurements, which assumed sphericity of particles. Thus averaging of axis dimensions of the platy particles likely skews the particle-size distributions.

X-ray diffraction spectra of colloidal material were interpreted to show the presence of kaolinite, illite, vermiculite, dioctahedral vermiculite, and trace amounts of chlorite. Quartz peaks were absent or barely distinguishable from background.

WDCs were notably enriched in some elements (Al, Fe, Ga, Rb) and others were relatively excluded (Si,Ti, Hf, Zr) compared to soil and shale parent material (Table 1, Appendix 1). The settling tests segregated 16–23% of WDC mass into material that settled after 21 h, 27–41% settled after 96 h, and 41–50% remained in suspension after 96 h. However, segregation of WDCs by settling did not generate pronounced geochemical differences (Table 1) with two exceptions. Zirconium and Ti concentrations were slightly lower in WDCs still in suspension after 96 h compared to WDCs that settled after 21 or 96 h. Greater Mn concentrations in the WDCs compared to the soils or settling test WDCs (Table 1) are likely an artifact resulting from atmospheric deposition adding Mn to surface soils (Herndon et al., 2011) and the exclusion of surface samples from the settling tests.

Concentrations of elements in the dissolved (< 3 kDa) fraction of the WDC suspensions varied widely (Table 2). Elements like Ca, K, Mn, and P had high concentrations that accounted for > 1% of the element in suspension. Most other elements had lower concentrations and generally accounted for tenths or hundredths of a percent of the total in suspension. A pattern of greater fractions in the < 3 kDa fraction in samples collected at or closer to the surface is observed across all of the elements.

Table 1
Concentrations (average and range) of major and select trace elements in WDCs extracted from soils and from the WDC settling tests. Compositions of shale parent material and bulk soil from Jin et al. (2010) and Ma et al. (2011a) are included for comparison. Composition data for individual WDC samples are provided in Appendix 1.

	Al	Ca	Fe	K	Mg	Mn	P	Si	Ti
	(%)	(%)	(%)	(%)	(%)	(%)	(%)	(%)	(%)
Bulk WDCs	13.3	0.14	6.4	3.2	0.8	0.22	0.11	na[a]	0.34
(n = 8)	12.2–14.0	0.07–0.27	5.7–7.5	2.3–4.2	0.7–0.9	0.03–0.69	0.04–0.21		0.28–0.39
WDCs 21 h	13.6	0.10	6.2	4.8	0.8	0.05	0.12	20.3	0.45
Settled (n = 1)									
WDCs 96 h	13.3	0.11	6.6	4.4	0.9	0.06	0.08	20.4	0.45
Settled (n = 4)	13.1–13.7	0.05–0.20	6.1–7.1	3.6–5.0	0.8–1.0	0.03–0.09	0.04–0.11	19.9–21.0	0.38–0.52
WDCs 96 h	13.9	0.16	7.0	4.4	0.8	0.07	0.08	19.2	0.26
Suspended (n = 4)	13.6–14.3	0.05–0.3	6.5–7.9	3.6–5.1	0.8–1.0	0.04–0.12	0.03–0.13	18.7–19.6	0.22–0.30
Drill core, parent	10.7	0.12	5.5	3.8	0.9	0.08	0.06	26.7	0.64
Material (n = 12)	9.8–11.3	0.09–0.14	5.3–6.0	3.5–4.0	0.9–1.1	0.02–0.18	0.04–0.07	25.9–27.3	0.57–0.67
Soils	7.9	0.11	4.0	2.5	0.6	0.13	0.07	30.1	0.65
(n = 16)	5.3–10.3	0.06–0.17	2.5–5.2	1.6–3.5	0.4–0.9	0.05–0.46	0.03–0.13	26.9–32.9	0.61–0.71

	Ga	Gd	Hf	La	Lu	Rb	Th	U	Zr
	(ppm)	(ppm)	(ppm)	(ppm)	(ppm)	(ppm)	(ppm)	(ppm)	(ppm)
WDCs	40	4.2	3.8	40	0.4	263	13.9	3.0	129
(n = 8)	38–43	2.5–6.9	3–5	26–51	0.3–0.6	232–299	11.0–17.1	2.3–4.5	97–156
WDCs 21 h	38	6.0	5	63	0.6	274	18.7	3.7	156
Settled (n = 1)									
WDCs 96 h	37	5.9	4.3	56	0.5	263	18	3.9	142
Settled (n = 4)	34–38	4.9–8.8	4–5	51–68	0.4–0.7	252–280	17–21	3.3–5.1	128–158
WDCs 96 h	37	4.5	4	34	0.5	264	15	3.7	128
Suspended (n = 4)	34–39	3.7–6.7	4	29–37	0.4–0.7	247–281	14–16	3.2–4.5	116–137
Drill core, parent	26	7.3	5.3	51	0.7	209	15.3	3.3	178
Material (n = 12)	24–29	6.4–8.1	5–6	46–57	0.5–2.5	187–228	14.2–16.8	3.1–3.6	155–203
Soils	18	5.3	7.4	41	0.5	142	12.1	3.4	270
(n = 16)	13–25	4.6–6.7	5–9	37–50	0.4–0.6	99–199	10.4–14.8	2.9–3.7	182–351

[a] Not available. Silicon was not an approved analyte for the method at the time of analysis.

Table 2
Concentrations of major and select trace elements in the < 3 kDa fraction of suspensions from the WDC extractions. The fraction of each element in the < 3 kDa fraction relative to the total WDC suspension is listed in the bottom panel. Where concentrations were below reporting limits shown, a value equal to half the reporting limit was used to calculate the fraction.

Sample	Al	Ca	Fe	K	Mg	Mn	P	Ti	Ga	La	Rb	Zr
	(μg/L)	(μg/L)	(μg/L)	(μg/L)	(μg/L)	(μg/L)	(μg/L)	(μg/L)	(μg/L)	(μg/L)	(μg/L)	(μg/L)
SRT 0–10 cm	221	100	14	680	80	718	90	< 1	< 0.06	0.13	0.99	0.3
SRT 20–25 cm	13	40	< 10	400	10	8	50	< 1	< 0.06	< 0.02	0.53	< 0.1
SMS 0–10 cm	159	200	18	490	50	692	40	< 1.5	< 0.09	0.16	0.7	0.3
SMS 20–30 cm	52	40	17	360	20	58	< 20	< 1	< 0.06	0.04	0.73	0.3
SMS 30–40 cm	44	70	12	480	30	77	< 20	< 1	< 0.06	0.1	0.88	0.84
SVF 0–10 cm	196	90	58	520	80	236	< 20	< 1	< 0.06	0.05	0.87	0.4
SVF 40–50 cm	7.2	70	< 10	200	70	7	< 20	< 1	< 0.06	< 0.02	0.49	< 0.1
SVF 90–100 cm	2.5	< 30	< 10	200	20	0.3	< 20	< 1	< 0.06	< 0.02	0.12	< 0.1
Fraction of WDC sample < 3 kDa												
SRT 0–10 cm	0.4%	15%	0.06%	6.5%	2.6%	29.2%	10.4%	0.04%	0.2%	0.8%	1.0%	0.7%
SRT 20–25 cm	0.01%	5%	0.01%	1.3%	0.2%	1.8%	5.8%	0.02%	0.1%	0.03%	0.2%	0.05%
SMS 0–10 cm	0.4%	42%	0.09%	5.9%	1.9%	29.2%	6.9%	0.07%	0.3%	1.4%	0.8%	0.8%
SMS 20–30 cm	0.1%	13%	0.07%	3.4%	0.7%	13.7%	2.0%	0.04%	0.2%	0.3%	0.8%	0.6%
SMS 30–40 cm	0.06%	18%	0.03%	2.8%	0.7%	15.3%	1.8%	0.02%	0.1%	0.2%	0.6%	0.5%
SVF 0–10 cm	0.5%	28%	0.3%	6.4%	3.0%	59.8%	4.7%	0.04%	0.2%	1.1%	1.0%	2.4%
SVF 40–50 cm	0.003%	3%	0.004%	0.4%	0.5%	1.5%	1.7%	0.01%	0.1%	0.02%	0.1%	0.02%
SVF 90–100 cm	0.003%	0.8%	0.01%	0.7%	0.3%	0.06%	1.9%	0.02%	0.1%	0.03%	0.1%	0.04%

3.2. Consideration of WDCs to represent colloids for modeling

Characteristics of the WDCs establish the rationale for using them to represent mobile colloidal material in soil for the purpose of modeling. Particle-size distributions for the WDCs (Fig. 2) are similar in biomodal distribution and particle diameter to those measured by Kaplan et al. (1997). That study found similarities between mobile colloids draining from two reconstructed pedons and water-dispersible clay isolated from those pedons.

The mineralogy of WDCs matches that of clay minerals present in bulk soil at SSHO, including kaolinite, illite, vermiculite, dioctahedral vermiculite and chlorite (Jin et al., 2010). Of these, only kaolinite is considered secondary due to its absence in parent shale. Other studies have noted mineralogical similarities between mobile colloids and the 0–2 μm fraction in soil (Cornu et al., 2014). The STEM images indicate some non-clay, crystalline minerals in the WDCs (Fig. 3). Quartz (36–63 wt%) and feldspar (1.2–6.6 wt%) are relatively abundant in bulk soil. Non-detection of quartz and feldspar in the WDCs by XRD suggests that they are present as particles > 1 μm. In contrast, Fe-oxides are sparse in bulk soil (0–2.5 wt%) and non-detection in the colloids may not indicate absence, or exclusion due to larger size, but simply presence below detection limits. Although the STEM images indicate some non-clay minerals are present in WDCs, XRD suggests they are a minor component. Thus, WDCs at SSHO generally reflect clay minerals inherited from parent shale plus kaolinite, and are mineralogically fractionated from bulk soil by general absence of quartz and feldspar. Such particle-size driven fractionation was previously assumed, and enrichment of bulk soil relative to shale parent material content of quartz (30–46 wt%) helped drive the conclusion that downslope loss of fine particles is an important process at SSHO (Jin et al., 2010).

Elemental data support the same general mineralogical fractionation. The average molar Si/Al ratio calculated for WDCs from the settling tests is 1.4 (Table 1). This value is similar to the ratio for ideal illite (1.8) and kaolinite (1.0), lower than the value of 2.4 calculated for shale parent material, and much lower than the value of 3.6 calculated for the quartz-enriched soil.

3.3. Tracer ratios for modeling

Differences in elemental compositions of WDCs, soil, and parent material are the basis for quantifying colloid movement using the dual-phase model. In the previous application of the model, the ratio Ti/Zr was used as the tracer, due to enrichment of Ti and depletion of Zr in WDCs derived from granitic materials, and practical insolubility of both elements (Bern et al., 2015). At SSHO, Ti and Zr are both partially excluded from colloids (Table 1), and the Ti/Zr ratio does not distinguish WDCs from soil (Table 3). Therefore, other practically insoluble elements were appraised for use as tracers.

Scatterplots of centered logratio transformed elemental data identify potential tracer elements that behave similarly at SSHO with regards to weathering and partitioning into colloids. These include Al, Ga, and Rb (compared pairwise) and Zr and Hf (Fig. 4). Similar behavior during weathering, particularly with regards to mobility, is indicated by tight linear correlation from parent shale to soil and suggests no preferential loss of one element versus the other. Similar partitioning into WDCs by different elements is indicated by the position of the WDC data along the same linear trends. Underlying all such correlations is a parent material of relative geochemical homogeneity, as suggested by the relatively tight clustering of shale data. Similarity of behavior in the weathering environment between these elements can also be seen through the similarity of their mass ratios between WDCs, soil, and parent shale (Table 3).

Relative enrichment of WDCs in Al, Ga, and Rb positions them above parent shale along their correlation lines (Fig. 4). The loss of WDCs from soil shifts soil below parent shale for these three elements, but along the same correlation lines. Relative depletion of WDCs in Zr and Hf causes an opposite pattern along their correlation line. Practical insolubility is also necessary to maintain the tight linear correlations observed. Substantial losses of any of these elements by solution would likely shift affected samples off of the linear trend line, or cause notable differences in their mass ratios (Table 3) because dissolution rarely affects two elements identically.

A number of factors drive low solubility for the tracer elements. Practical insolubility is a hallmark of Zr in the weathering environment (Tole, 1985). Similar geochemical behavior between Zr and Hf is expected, as they have similar ionic radii which allows Hf to substitute for Zr in Zr-bearing phases (Bau, 1996). Aluminum concentrations in soil

Table 3
Ratios of elements used as tracers in the dual-phase mass balance model (see Fig. 5), and ratios of elements that associate similarly in weathering products (see Fig. 4). Compositions of shale parent material and bulk soil from Jin et al. (2010) and Ma et al. (2011a) are included for comparison. Ratios marked with an asterisk are multiplied by 10^{-3}.

	Tracer ratios						Similar associations				
	Al/Zr	Ga/Zr	Rb/Zr	Al/Hf*	Ga/Hf	Rb/Hf	Al/Ga*	Al/Rb	Ga/Rb	Zr/Hf	Ti/Zr
Bulk WDCs	1056	0.32	2.1	36	11	71	3.3	509	0.15	34	27
(n = 8)	865–1263	0.26–0.39	1.9–2.5	27–44	8–13	58–81	3.2–3.6	467–547	0.14–0.17	31–37	21–37
WDCs 21 h Settled (n = 1)	872	0.24	1.8	27	8	55	3.6	496	0.14	31	29
WDCs 96 h	949	0.26	1.9	32	9	63	3.7	507	0.14	33	32
Settled (n = 4)	835–1039	0.23–0.29	1.7–2.1	26–34	7–10	53–70	3.4–3.9	489–528	0.13–0.15	32–37	29–34
WDCs 96 h	1092	0.29	2.1	35	9	66	3.7	527	0.14	32	20
Suspended (n = 4)	1015–1172	0.27–0.31	2.0–2.2	34–36	9–10	62–70	3.5–4.0	509–551	0.14–0.15	29–34	17–23
Drill core, parent	608	0.15	1.2	20	5	39	4.1	516	0.13	33	36
Material (n = 12)	485–710	0.12–0.17	1.0–1.3	16–23	4–5	33–45	3.7–4.5	471–552	0.12–0.13	31–36	30–40
Soils	315	0.07	0.6	11	3	20	4.3	559	0.13	37	25
(n = 16)	151–561	0.04–0.13	0.3–1.0	6–20	1–5	11–37	3.9–4.6	511–587	0.12–0.14	32–40	20–33

pore water and stream water at SSHO are extremely low and the pore-water pH range of 3.5–5.5 also suggests limited Al mobility in solution (Jin et al., 2011; Sullivan et al., 2016a). Gallium mimics the behavior of Al in solution and substitutes for Al in Al-bearing phases (Bénézeth et al., 1997; Goldsmith, 1950). Associations between Ga and Al can be maintained even under intense weathering, similar to Zr and Hf (Horbe and da Costa, 1999) and Ga/Al ratios are quite similar across materials at SSHO (Table 3). In contrast, low solubility and similar weathering behavior between Rb and Al or Ga might be unexpected. However, Rb often substitutes for K in K-bearing phases, and illite is the likely predominant host for Rb at SSHO. Furthermore, Rb sorbs more strongly than K and is therefore likely to be better retained in the interlayer spaces of illite (Horstman, 1957). The linear correlations of Rb with both Al and Ga (Fig. 4), and similar ratios of Al/Rb and Ga/Rb across weathering products (Table 3), indicate similar practical insolubility for all three elements.

Having established practical insolubility for the above elements, the contrasting behavior of WDC-associated elements (Al, Ga, Rb) and those partially excluded from WDCs (Zr, Hf) may be observed in a second set of scatterplots (Fig. 5). Loss of WDCs, with their distinctive

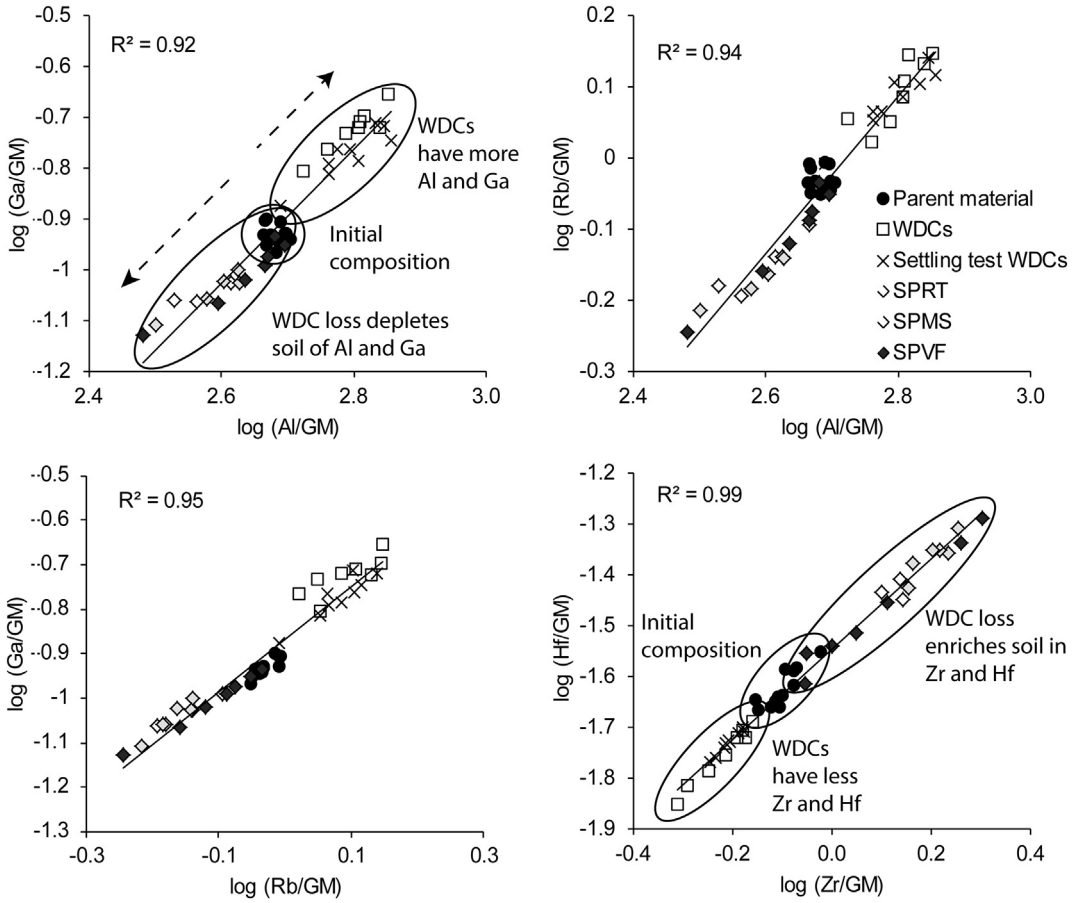

Fig. 4. Plots of Al versus Ga, Al versus Rb, Rb versus Ga, and Zr versus Hf in SSHO materials. Soils are SPRT (ridgetop), SPMS (middle slope), and SPVF (valley floor). Element concentrations have undergone a centered logratio transformation using the geometric mean (GM). Elements compared pairwise here behave similarly to each other at SSH with regards to both chemical weathering and partitioning between larger and smaller particles. Squares of correlation coefficients and trend lines included for reference, all correlations have $p < 0.001$.

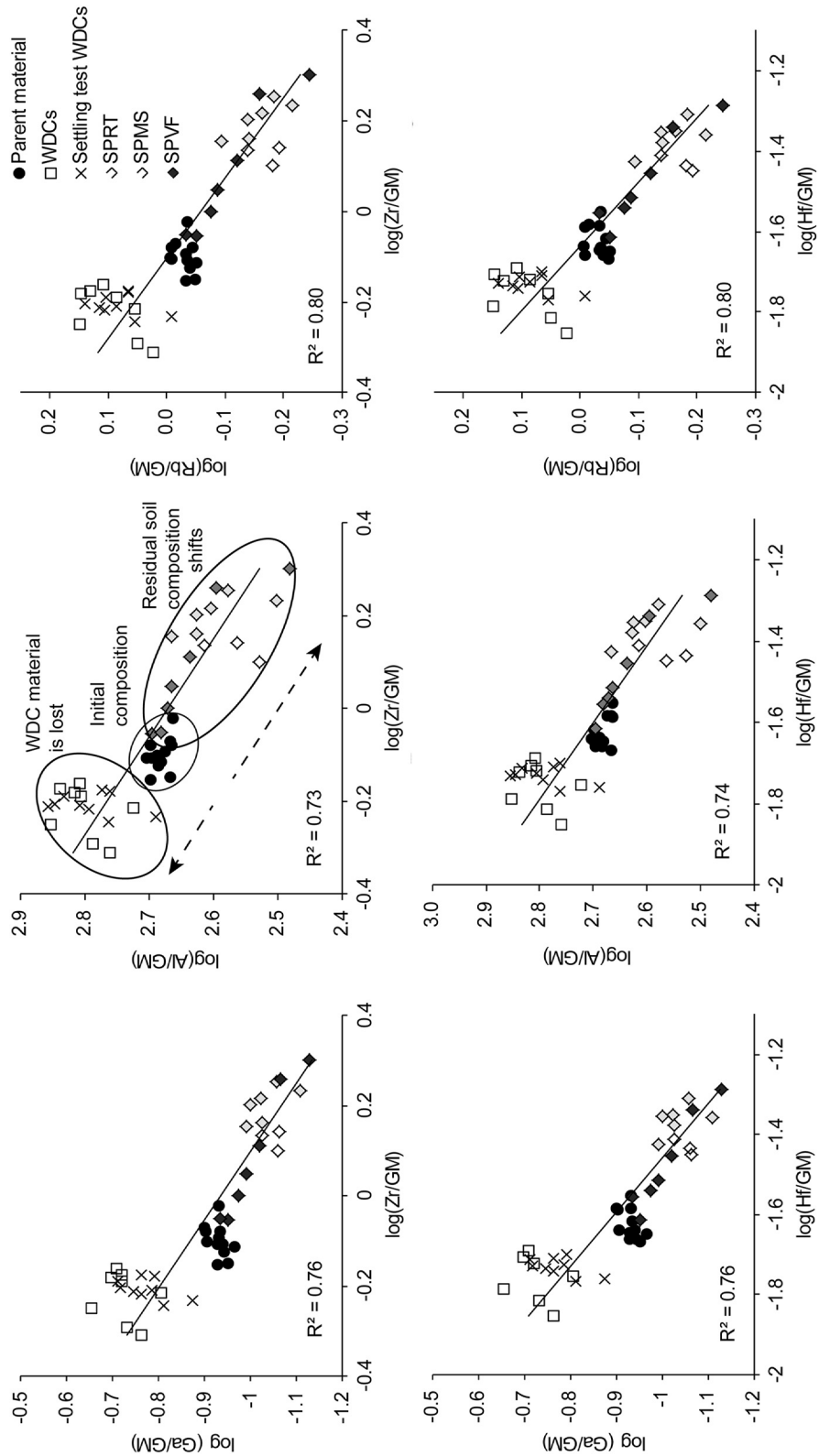

Fig. 5. Plots of Zr versus Ga, Al, and Rb (individually) and Hf versus Ga, Al, and Rb (individually). Element concentrations have undergone a centered logratio transformation using the geometric mean (GM). Elements compared pairwise here are relatively insoluble at SSHO and partition differently into the WDC fraction. As illustrated with Zr versus Al, the loss of WDCs from soil has shifted soil composition relative to the parent material samples on the plots. Squares of correlation coefficients and trend lines included for reference, all correlations have $p < 0.001$.

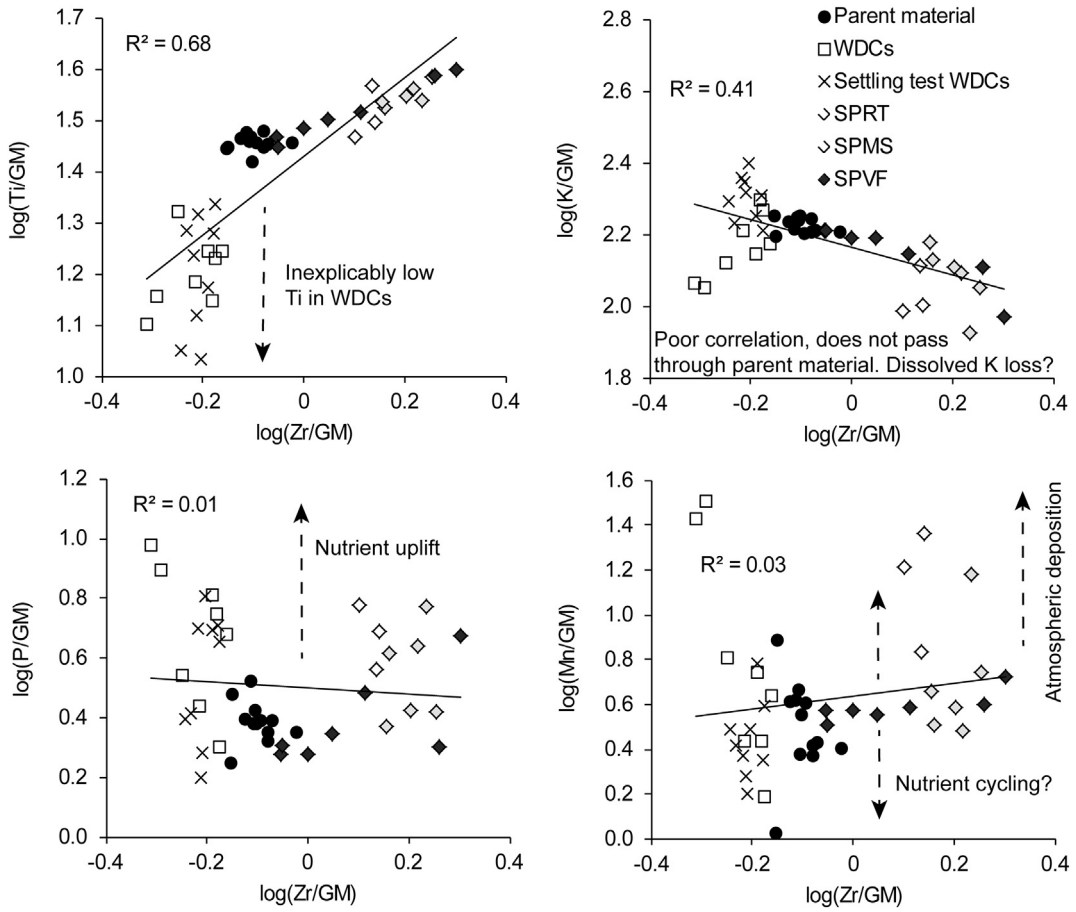

Fig. 6. Plots of Ti, K, P, and Mn versus Zr in SSHO materials. Element concentrations have undergone a centered logratio transformation using the geometric mean (GM). Squares of correlation coefficients and trend lines included for reference.

composition relative to these elements, drives opposing changes in the elemental composition of soil. Certain soil samples fall further from the correlation line, suggesting some minor influence other than WDC loss. The scatter observable in the WDC compositions, compared to the shale parent material, indicates WDC compositions as a greater source of uncertainty in subsequent modeling.

Other sources of uncertainty regarding the suitability of tracer elements for quantifying WDC losses include the degree to which they are affected by partial solubility, atmospheric inputs, biological cycling, or other processes. Useful perspective may be gained from examining similar scatterplots for elements affected by such processes (Fig. 6). Greater solubility and biological cycling of K relative to Rb is observable in poorer correlation between K and Zr, and a correlation that passes more through the edge shale parent material composition cluster. Manganese is an element for which substantial modern atmospheric deposition has been documented at SSHO (Herndon et al., 2011). Such external additions are one reason for elevation of many soil and WDC points high above any correlation line between Mn and Zr. Cycling of Mn as a nutrient and the influence of redox on Mn mobility may also play roles in generating scatter. Zinc is also an element for which the modern atmospheric deposition flux outstrips the soil production flux severalfold (Kraepiel et al., 2015). As a result many soil and WDC points plot above the correlation line for Zn (plot not shown). Phosphorus is not substantially affected by atmospheric deposition at SSHO, but it is heavily biologically cycled (Kraepiel et al., 2015). Many points plotting above parent material suggest P uplift from depth and/or retention in soil organic matter. Low Ti concentrations in the WDCs pull them off a trend defined by parent material and soil. Although the underlying process is unclear, this illustrates Ti as a poor tracer of WDC movement. Distortion in all these relationships contrasts with the relatively straightforward relationships between Al, Ga, Rb, Hf, and Zr (Fig. 5).

3.4. Dual-phase mass balance modeling

Distinctions between parent shale, soil, and WDCs for the ratios Al/Zr, Ga/Zr, Rb/Zr, Al/Hf, Ga/Hf, and Rb/Hf indicated their suitability as tracers of WDC movement (Table 3). All six ratios were used to quantify WDC losses from SSHO soils via the dual-phase model (Bern et al., 2015). The advantage of using six ratios involving five elements is that uncertainty and error associated with the individual elements can partially cancel out. Elemental compositions of shale parent material and soil from previous studies were used (Jin et al., 2010; Ma et al., 2013). Soil samples were not sieved prior to analysis and therefore accounting for a separate gravel (> 2 mm) fraction was unnecessary. As the WDC settling tests produced little to no geochemical fractionation (Tables 1, 3; Figs. 4, 5), all WDC data were lumped together for modeling. Proportional mass change results are reported here. For example, the mass of WDCs (M_c) was divided by the mass of parent material as (M_p) to give the percentage mass loss via WDCs. Output was generated using each tracer ratio individually, and uncertainty for total mass changes was propagated through the model as standard errors of average tracer element concentrations in parent shale and WDCs (Bern et al., 2015). Output from each tracer ratio was similar and generally overlapped within uncertainty. Results were therefore averaged for all six ratios.

The magnitudes of WDC mass losses are great, ranging up to 68 ± 7% (Table 4). WDC mass losses in excess of 50% are detected at the surface of each profile, increase with progression down the slope, and exhibit little variability with depth. Such a pattern suggests

Table 4
Mass changes in soil relative to starting parent material due to colloidal redistribution (M_c/M_p) and solutional processes (M_d/M_p), as determined by the dual-phase model. Each value represents the averaged output from modeling with the six element pairs described in the text. Uncertainty reflects the standard error for parent material and WDC composition, propagated through the modeling, and averaged for the six element pairs.

Sample	M_c/M_p	M_d/M_p	$M_c/(M_c + M_d)$
SPRT 00–10	− 58 ± 6%	− 2 ± 2%	97%
SPRT 10–20	− 58 ± 6%	− 5 ± 2%	92%
SPRT 20–30	− 56 ± 6%	− 1 ± 2%	99%
SPMS 00–10	− 65 ± 6%	− 7 ± 2%	90%
SPMS 10–20	− 64 ± 6%	− 6 ± 2%	91%
SPMS 20–30	− 61 ± 6%	− 4 ± 2%	93%
SPMS 30–40	− 60 ± 6%	− 5 ± 2%	93%
SPMS 40–50	− 58 ± 6%	− 5 ± 2%	92%
SPMS 50–59	− 53 ± 6%	− 4 ± 2%	94%
SPVF 00–10	− 68 ± 7%	− 5 ± 2%	93%
SPVF 10–20	− 63 ± 6%	− 5 ± 2%	93%
SPVF 20–30	− 53 ± 6%	− 3 ± 2%	94%
SPVF 30–40	− 43 ± 6%	1 ± 2%	102%
SPVF 40–50	− 36 ± 6%	0 ± 2%	99%
SPVF 50–60	− 15 ± 5%	6 ± 1%	164%
SPVF 60–67	− 23 ± 5%	− 2 ± 1%	94%

continued WDC losses as bulk soils move from upslope to downslope. WDC losses are notably smaller in deeper portions of the valley floor profile, likely reflecting gains of WDCs mobilized from the slopes above. Mass losses via solution are comparatively small, ranging from 7 ± 2% up to a gain of 6 ± 1% in a single deeper sampling increment of a valley floor profile (Table 4). Mass transfer coefficients for individual elements are listed in Tables 5A,B. Adding the coefficient for an element j for WDCs ($\tau_{j,c}$) to that for element j in dissolved form ($\tau_{j,d}$) yields the total mass transfer coefficient ($\tau_{j,c+d}$). Mass losses of all elements considered were greater via WDCs than via solution, but showed substantial element to element variability as discussed below. The small solution losses and gains calculated for Zr and the other tracer elements are a byproduct of averaging results from multiple tracer ratios. Per the formulation of the model, which assumes insolubility of tracer elements, solution losses of Ga and Zr would be zero when using Ga/Zr as the tracer, but other ratios like Al/Hf can and do indicate Ga and Zr solution losses. Such losses are small across the tracer elements though (− 0.06 to + 0.05), and could reflect both natural heterogeneity and analytical uncertainty as much as violation of the assumption of negligible solubility for the tracer elements.

4. Discussion

4.1. Colloid mass losses dominate soil development

The dual-phase model shows that losses of colloidal material dominate the development of SSHO soils. Dividing colloidal mass loss (M_c) by the combination of colloidal and dissolved mass losses ($M_c + M_d$), the dual-phase model indicates that WDCs account for at least 90% of the actual mass lost from every sampling increment (Table 4). Losses of Zr indicate that quantifications of mass and element losses that used Zr as an index were systematically skewed. Total mass transfer coefficients for Zr ($\tau_{c+d,Zr}$) ranged from − 0.08 to − 0.47, with a median of − 0.41, which indicates a loss of 41% of the Zr relative to that inherited from parent material (Table 5B). These two findings offer new perspective on the development of soils at SSHO and, by extension, other soils derived from sedimentary rocks.

Zirconium, and the assumption of its immobility, underpins calculations used to distinguish between the chemical weathering rate (W) and erosion rate (E) as they contribute to the total denudation rate (D). In settings assumed to be at steady state, such as SSHO (Jin et al., 2010), W and E compose D, which is in balance with the soil production rate (P):

$$P = D = W + E \tag{13}$$

The term chemical depletion fraction (CDF) has been defined as the fraction of chemical weathering relative to the total denudation rate, and it may be calculated using concentrations of an index element, generally Zr (Riebe et al., 2003):

$$CDF = \frac{W}{D} = 1 - \frac{C_{Zr,p}}{C_{Zr,s}} \tag{14}$$

Here $C_{Zr,p}$ and $C_{Zr,s}$ are the concentrations of Zr in parent material and regolith (soil), respectively. The degree to which concentrations of Zr in regolith are greater than those in parent material are understood to reflect mass loss by chemical weathering (dissolution). If Zr has been lost from regolith, however, the CDF will be underestimated. The losses of Zr via WDCs indicate that is the case at SSHO. Such underestimation can be addressed by using results from the dual-phase model.

Table 5A
Values of mass transfer coefficients for both the colloidal (WDC) component ($\tau_{j,c}$) and the dissolved component ($\tau_{j,d}$) for major elements in SSHO soils. The two components can be summed to determine the total mass transfer coefficient.

Depth	Al		Ca		Fe		K		Mg		Mn		P		Si		Ti	
(cm)	$\tau_{Al,c}$	$\tau_{Al,d}$	$\tau_{Ca,c}$	$\tau_{Ca,d}$	$\tau_{Fe,c}$	$\tau_{Fe,d}$	$\tau_{K,c}$	$\tau_{K,d}$	$\tau_{Mg,c}$	$\tau_{Mg,d}$	$\tau_{Mn,c}$	$\tau_{Mn,d}$	$\tau_{P,c}$	$\tau_{P,d}$	$\tau_{Si,c}$	$\tau_{Si,d}$	$\tau_{Ti,c}$	$\tau_{Ti,d}$
SPRT																		
0–10	− 0.73	0.00	− 0.69	0.11	− 0.70	− 0.03	− 0.60	− 0.19	− 0.51	− 0.28	− 1.04	2.37	− 1.04	0.77	− 0.43	− 0.16	− 0.32	− 0.29
10–20	− 0.73	− 0.02	− 0.69	0.23	− 0.69	− 0.04	− 0.59	− 0.20	− 0.50	− 0.28	− 1.03	1.72	− 1.04	0.92	− 0.43	− 0.17	− 0.32	− 0.31
20–30	− 0.71	0.00	− 0.68	− 0.10	− 0.67	0.01	− 0.58	− 0.16	− 0.49	− 0.24	− 1.00	0.68	− 1.01	0.55	− 0.42	− 0.08	− 0.31	− 0.24
SPMS																		
0–10	− 0.81	− 0.02	− 0.77	0.14	− 0.77	− 0.07	− 0.66	− 0.21	− 0.56	− 0.31	− 1.15	1.28	− 1.16	0.78	− 0.48	− 0.20	− 0.36	− 0.32
10–20	− 0.80	− 0.01	− 0.77	− 0.01	− 0.76	− 0.06	− 0.66	− 0.18	− 0.56	− 0.29	− 1.14	0.52	− 1.15	0.41	− 0.48	− 0.16	− 0.36	− 0.32
20–30	− 0.77	0.00	− 0.73	0.06	− 0.73	− 0.05	− 0.63	− 0.17	− 0.53	− 0.27	− 1.09	0.33	− 1.09	0.59	− 0.45	− 0.13	− 0.34	− 0.31
30–40	− 0.75	0.00	− 0.71	− 0.04	− 0.71	− 0.03	− 0.61	− 0.17	− 0.52	− 0.25	− 1.06	0.38	− 1.06	0.39	− 0.44	− 0.14	− 0.33	− 0.32
40–50	− 0.73	0.01	− 0.70	0.01	− 0.69	− 0.02	− 0.59	− 0.15	− 0.50	− 0.24	− 1.03	0.33	− 1.04	0.58	− 0.43	− 0.13	− 0.32	− 0.31
50–59	− 0.67	0.01	− 0.64	− 0.14	− 0.63	− 0.01	− 0.54	− 0.13	− 0.46	− 0.22	− 0.95	0.42	− 0.95	0.26	− 0.40	− 0.11	− 0.30	− 0.27
SPVF																		
0–10	− 0.85	− 0.02	− 0.81	0.16	− 0.81	− 0.07	− 0.69	− 0.19	− 0.59	− 0.31	− 1.20	0.53	− 1.21	0.61	− 0.50	− 0.17	− 0.38	− 0.33
10–20	− 0.79	0.00	− 0.75	0.06	− 0.75	− 0.05	− 0.64	− 0.16	− 0.55	− 0.27	− 1.12	0.41	− 1.13	0.30	− 0.47	− 0.15	− 0.35	− 0.31
20–30	− 0.66	0.01	− 0.63	0.12	− 0.63	− 0.05	− 0.54	− 0.13	− 0.46	− 0.21	− 0.94	0.37	− 0.94	0.42	− 0.39	− 0.11	− 0.29	− 0.26
30–40	− 0.54	0.03	− 0.52	0.06	− 0.51	− 0.02	− 0.44	− 0.09	− 0.37	− 0.15	− 0.76	0.28	− 0.77	0.19	− 0.32	− 0.07	− 0.24	− 0.20
40–50	− 0.45	0.03	− 0.45	0.13	− 0.43	− 0.02	− 0.37	− 0.09	− 0.31	− 0.11	− 0.64	0.27	− 0.64	0.11	− 0.27	− 0.05	− 0.20	− 0.17
50–60	− 0.19	0.05	− 0.20	0.11	− 0.18	0.01	− 0.16	− 0.03	− 0.13	− 0.01	− 0.27	0.17	− 0.28	− 0.07	− 0.11	0.05	− 0.09	− 0.06
60–67	− 0.29	0.01	− 0.30	− 0.02	− 0.28	− 0.01	− 0.24	− 0.06	− 0.20	− 0.06	− 0.41	0.08	− 0.41	− 0.04	− 0.17	− 0.07	− 0.13	− 0.16

Table 5B
Values of mass transfer coefficients for both the colloidal (WDC) component ($\tau_{j,c}$) and the dissolved component ($\tau_{j,d}$) for trace elements in SSHO soils. The two components can be summed to determine the combined mass transfer coefficient.

Depth	Ga		Gd		Hf		La		Lu		Rb		U		Th		Zr	
(cm)	$\tau_{Ga,c}$	$\tau_{Ga,d}$	$\tau_{Gd,c}$	$\tau_{Gd,d}$	$\tau_{Hf,c}$	$\tau_{Hf,d}$	$\tau_{La,c}$	$\tau_{La,d}$	$\tau_{Lu,c}$	$\tau_{Lu,d}$	$\tau_{Rb,c}$	$\tau_{Rb,d}$	$\tau_{U,c}$	$\tau_{U,d}$	$\tau_{Th,c}$	$\tau_{Th,d}$	$\tau_{Zr,c}$	$\tau_{Zr,d}$
SPRT																		
0–10	−0.79	0.02	−0.38	−0.35	−0.44	−0.04	−0.49	−0.20	−0.48	−0.20	−0.74	−0.02	−0.61	−0.04	−0.59	−0.13	−0.44	0.05
10–20	−0.78	0.03	−0.38	−0.34	−0.44	−0.01	−0.49	−0.19	−0.48	−0.17	−0.73	−0.01	−0.61	−0.02	−0.58	−0.12	−0.43	0.01
20–30	−0.76	0.02	−0.37	−0.35	−0.42	−0.01	−0.48	−0.20	−0.47	−0.20	−0.71	−0.02	−0.59	−0.02	−0.57	−0.11	−0.42	0.01
SPMS																		
0–10	−0.87	0.03	−0.42	−0.36	−0.49	−0.04	−0.55	−0.20	−0.54	−0.18	−0.82	−0.01	−0.68	−0.02	−0.65	−0.13	−0.48	0.04
10–20	−0.86	0.03	−0.42	−0.37	−0.48	−0.02	−0.54	−0.19	−0.53	−0.18	−0.81	−0.02	−0.67	−0.03	−0.64	−0.13	−0.48	0.02
20–30	−0.82	0.03	−0.40	−0.38	−0.46	−0.02	−0.52	−0.22	−0.51	−0.19	−0.77	−0.02	−0.64	−0.01	−0.61	−0.13	−0.46	0.03
30–40	−0.80	0.03	−0.39	−0.37	−0.45	−0.02	−0.50	−0.22	−0.50	−0.19	−0.75	−0.02	−0.62	0.01	−0.60	−0.13	−0.45	0.02
40–50	−0.78	0.02	−0.38	−0.37	−0.44	−0.01	−0.50	−0.21	−0.49	−0.20	−0.73	−0.02	−0.61	0.03	−0.58	−0.12	−0.43	0.01
50–59	−0.72	0.00	−0.35	−0.35	−0.40	−0.04	−0.45	−0.21	−0.44	−0.19	−0.67	−0.02	−0.56	0.01	−0.53	−0.12	−0.40	0.04
SPVF																		
0–10	−0.91	0.04	−0.44	−0.36	−0.51	−0.03	−0.57	−0.20	−0.56	−0.18	−0.86	−0.02	−0.71	−0.01	−0.68	−0.13	−0.51	0.04
10–20	−0.85	0.02	−0.41	−0.36	−0.47	−0.04	−0.53	−0.21	−0.52	−0.18	−0.80	−0.02	−0.66	−0.02	−0.63	−0.13	−0.47	0.05
20–30	−0.71	0.00	−0.34	−0.33	−0.40	−0.03	−0.45	−0.19	−0.44	−0.18	−0.67	−0.02	−0.55	−0.01	−0.53	−0.12	−0.39	0.03
30–40	−0.58	−0.02	−0.28	−0.28	−0.32	−0.03	−0.37	−0.14	−0.36	−0.12	−0.54	−0.01	−0.45	0.04	−0.43	−0.09	−0.32	0.03
40–50	−0.48	−0.02	−0.24	−0.23	−0.27	−0.01	−0.32	−0.10	−0.31	−0.08	−0.46	−0.01	−0.38	0.05	−0.36	−0.12	−0.27	0.01
50–60	−0.21	−0.06	−0.11	−0.09	−0.12	−0.03	−0.14	0.00	−0.14	−0.06	−0.19	−0.01	−0.16	0.14	−0.15	−0.06	−0.12	0.04
60–67	−0.31	−0.03	−0.16	−0.16	−0.17	0.02	−0.21	−0.06	−0.21	−0.09	−0.29	0.01	−0.24	0.10	−0.23	−0.04	−0.17	−0.02

The concentration of Zr that would have been present in a given volume of regolith if a fraction of the Zr inherited from parent material had not been lost via WDCs ($C^*_{Zr,s}$) can be calculated:

$$C^*_{Zr,s} = C_{Zr,s}(1 + \tau_{Zr,c+d})^{-1} \quad (15)$$

where $\tau_{Zr,c+d}$ is the overall mass transfer coefficient for Zr (Table 6). The value of $C^*_{Zr,s}$ may then be substituted into Eq. (14) for $C_{Zr,s}$ to obtain a CDF not skewed by Zr losses. The CDF calculated (Eq. (14)) for the ridge top soil profile by Jin et al. (2010) using a density- and thickness-weighted average Zr concentration of 263 ppm was 0.3. Using the same weighting calculation but substituting the $C^*_{Zr,s}$ for each sampling thickness gives an profile average Zr concentration of 447 ppm and a CDF of 0.6. This change from a CDF of 0.3 to 0.6 is a change in favor of weathering over erosion and is a result of correcting for the mobility of Zr. However, a CDF of 0.6 is similar to that of granitic regolith formed under a much warmer and wetter tropical climate (MAT = 22 °C; MAP = 420 cm) at Rio Iacos, Puerto Rico (Riebe et al., 2004), location of the fastest documented weathering rates of silicate rocks on the Earth's surface (White et al., 1998). The chemical weathering rate of shale-derived regolith under a temperate climate at SSHO should be much slower and, as explained below, it is slower.

Table 6
Measured concentrations of Zr in regolith compared to concentration of Zr that would have been present in regolith if a fraction of the Zr inherited from parent material had not been lost via WDCs ($C^*_{Zr,s}$) as calculated using Eq. (15).

Sample	$c_{Zr,s}$	$c^*_{Zr,s}$
	(ppm)	(ppm)
SPRT 00–10	273	452 ± 53
SPRT 10–20	275	480 ± 17
SPRT 20–30	246	416 ± 18
SPMS 00–10	351	634 ± 68
SPMS 10–20	329	606 ± 41
SPMS 20–30	295	519 ± 40
SPMS 30–40	288	502 ± 31
SPMS 40–50	277	482 ± 17
SPMS 50–59	266	417 ± 43
SPVF 00–10	349	660 ± 67
SPVF 10–20	318	556 ± 67
SPVF 20–30	258	407 ± 33
SPVF 30–40	219	310 ± 26
SPVF 40–50	208	280 ± 14
SPVF 50–60	182	199 ± 24
SPVF 60–67	191	237 ± 14

The chemical weathering rate (W) refers to all mass lost relative to bulk soil. It is therefore composed of both mass lost in true solution by chemical weathering, as well as mass lost as colloids. It has been implicitly assumed that colloidal losses in most cases are a small fraction of losses via solution, and that such losses are accounted for by traditional mass balance. However, the dual-phase model indicates that losses of colloidal material are large for SSHO (Table 4). The colloidal losses are conceptually difficult, particularly at SSHO, because mineralogy indicates that much of the colloidal component is clays inherited from shale that mix with secondary phases like kaolinite generated by chemical weathering. Therefore, physical rather than chemical weathering in regolith drives the generation of much colloidal material at SSHO. However, the colloids are appropriately part of the W component, as they are mobile relative to bulk soil. Mobility of the bulk soil is accounted for by the erosion rate (E). A solution to the conceptual difficulty is to drop the chemical qualifier and define W more broadly as the weathering rate. As indicated above, WDCs account for at least 90% of the mass lost from every depth increment of soil sampled (Table 4). Therefore, at SSHO, the *chemical* depletion fraction (CDF) described by the ratio W/D (Eq. (14)) is better understood as a *weathering* depletion fraction.

Removal of mass via colloidal material also contributes to volumetric collapse of the soil profile. However, the loss of Zr via colloids causes that collapse to be underestimated. Strain ($\varepsilon_{Zr,s}$) is a measure of such volumetric collapse (Brimhall et al., 1991), and it can be indexed to Zr by:

$$\varepsilon_{Zr,s} = \frac{V_s - V_p}{V_p} = \frac{\rho_p C_{Zr,p}}{\rho_s C_{Zr,s}} - 1 \quad (16)$$

with variables defined as in Section 2.3. Values of $\varepsilon_{Zr,s} > 0$ signify volumetric expansion and values < 0 signify volumetric collapse. Using measured concentrations of Zr from soil and the average from parent material, along with soil bulk density and a parent material bulk density of 2.85 g/cm^3 (Jin et al., 2010), strain values of −0.15, −0.16, and −0.23 are calculated for the 0–10 cm-, 10–20 cm-, and 20–30 cm-depth increments from the ridgetop SSHO soil, respectively. Substituting soil Zr concentrations corrected for Zr loss ($C^*_{Zr,s}$) by Eq. 15, the strain values for those same depth increments are −0.48, −0.52, and

− 0.54, respectively. The larger values, indicating approximately 50% volumetric collapse, reflect the substantial mass losses the SSHO soils have undergone (Table 4).

4.2. Consideration of colloid and Zr losses

It is a commonly assumed that zircons are the only host for Zr in soils and the parent materials from which soils are derived. Such assumptions have underpinned the use of Zr as an index element in weathering studies across the globe. However, the substantial concentrations of Zr (97–158 ppm) in the WDCs extracted here, even those allowed to settle for 96 h, indicate that Zr is present in a size fraction likely to be mobile in soil. Host phase mineralogy for Zr in this size fraction is unknown. Very fine-grained zircons may accompany clays during the erosion and deposition of material that becomes shale (Condie, 1991). The Zr-bearing phase in the fine-grained material need not all be zircon though. Zircons undergo solutional weathering (Tejan-Kella et al., 1991) and Zr-bearing, nanoscale material has now been identified in soils (Schindler and Hochella Jr, 2016). The fine grained nature of the Zr-bearing material is more important than its mineralogy, and that nature may contribute to substantial Zr mobility in soils derived from other fine-grained sedimentary rocks.

Although enhanced colloid losses in uppermost soils (Tables 4, 5A, B) suggest that processes at the surface dominate colloid removal, losses begin even before shale-derived material is incorporated into soil. Hasenmueller et al. (2017) describe weathered material collected from inside bedrock fractures below the soil in a catchment close to SSHO that is also underlain by the Rose Hill Formation. The weathered material is inferred to have formed in situ. The Al/Zr ratios of this material range from 275 to 576, and are lower than the Al/Zr ratios of Rose Hill Formation in that catchment (690) or at SSHO (608; Table 3). Such lower Al/Zr ratios suggest that the fracture material has undergone losses of colloidal material similar in composition to the WDCs from SSHO, which have high Al/Zr ratios that range from 865 to 1263. This illustrates that loss of Al-enriched colloidal material can be a part of incipient shale weathering, a point further demonstrated by greater quartz concentrations in the fracture material (Hasenmueller et al., 2017).

It is possible that WDC mass losses modeled here are overestimated. To the extent that Al, Ga, and Rb are more soluble than Zr and Hf at SSHO, some of the decreases in tracer ratios in soil relative to parent material (Table 3, Fig. 5) could be due to solution losses of those elements. Solution losses of Al, Ga, and Rb from the WDCs would shift their tracer ratios close to that of soil and parent material, driving overestimates of WDC mass losses to be quantified by the dual-phase model. However, the consistently tight correlations of WDCs and soil, with trends that pass through the composition of parent material, dispute this idea (Fig. 4). A more likely problem is potential discrepancies between WDCs isolated in the laboratory and colloids that have actually moved through the soil matrix during weathering and pedogenesis. Larger clay particles in the colloidal fraction can be physically filtered by the soil matrix (Noak et al., 2000; Seta and Karathanasis, 1997), but this may be less important in settings like SSHO with robust macropore flow. The extraction method employed here may have biased colloid composition in favor of inherited clay minerals at the expense of secondary mineral or organic colloids. More comparisons between WDCs dispersed from soils in the laboratory and mobile colloids in soils and streams would provide insight (Mills et al., 2017).

4.3. Colloidal and solutional losses of individual elements

As described above, Zr losses indicate systematic underestimates for weathering losses that were calculated using Zr as an index. Comparing the dual-phase model results to losses listed as mass transfer coefficients for the different depth increments in the same three soil profiles in Jin et al. (2010), the median additional losses of Al and Fe quantified here are 36% and 38%, respectively. For other elements the difference is even greater. Median additional losses of Ca and Si are 71% and 112% greater, respectively, than the results using Zr as an index. Median additional losses of Ti are 73% greater, but those for Mg and K are only 31% and 30% greater, respectively. Variability in these differences between elements is rooted in the proportions of the elements in the WDC fraction.

Beyond correcting for index element (Zr) mobility, the dual-phase model provides insight into how elements are lost from soil. It was previously concluded that Al and Fe were lost as colloids (Jin et al., 2010). The results here are confirmation, but suggest that clay minerals inherited from shale, rather than secondary phases formed in soil, drive much of that pattern. Iron isotopic compositions of WDCs from the settling tests suggest that WDCs contain a mixture of Fe unfractionated by weathering processes and isotopically fractionated Fe (Bern et al., 2017). Losses of the same inherited clays help drive Si losses via WDCs, but dissolved losses of Si are notable and likely reflect weathering of 2:1 clays like illite and vermiculized chlorite to kaolinite (Hasenmueller et al., 2017). Losses of elements like K, Mg, and Ca have been attributed entirely to mineral dissolution, but solution losses are now recognized to be fractions of total losses (Hasenmueller et al., 2017). The dual-phase model indicates that WDC losses actually account for the majority of K, Mg, and Ca losses, in contrast to a common assumption and documented patterns in other settings (Trostle et al., 2016). Potassium losses via WDCs may be linked to illite and Mg losses to chlorite. Unlike Mg and K, small solution gains of Ca are indicated at and near the surface of all three profiles. Phosphorus and Mn also have solution gains indicated, even at the ridge top where no contributions from upslope are possible. Atmospheric deposition from anthropogenic sources has driven substantial Mn accumulations in SSHO soils (Herndon et al., 2011) and those are tallied here as solution gains. The solution gains of Ca and P might reflect deposition of dust, which is also traced by the presence of feldspar in SSHO soils, despite feldspar absence for 6 m below the soil-bedrock interface (Jin et al., 2010). However, such gains could also reflect either nutrient uplift from roots penetrating below the soil zone (Kraepiel et al., 2015), or retention of nutrients by cycling through vegetation and soil biota, even as bulk soil and WDCs erode from the slope. The results for Ti are intriguing, as solution losses are proportionately greater than for Al or Fe, although Ti would generally be considered the least soluble of the three elements. Apparently there is a loss mechanism for Ti not associated with colloids as defined by the WDCs extracted here.

Losses of rare earth elements (REEs) display fractionation patterns as well as divisions between WDC and dissolved components that mesh with patterns in soil and soil water at SSHO. Losses of middle REEs, represented by total mass transfer coefficients of Gd, are 0.01–0.08 greater than those of the light or heavy REEs, represented by La and Lu, respectively (Table 5B), and match middle REE depletion patterns in SSHO soil (Ma et al., 2011b). However, dissolved losses of Gd are 0.04–0.19 greater than La and Lu, and these greater dissolved losses match a middle REE enrichment in soil- and stream waters that is sharper than the corresponding depletion in the hillslope soils (Ma et al., 2011b). As the WDC losses of light and heavy REEs exceed those of middle REEs, dissolution is indicated as the process driving the net fractionation pattern. In the case of U, WDC losses predominate, but a substantial amount of this U must be sorbed to account for isotopic fractionation and mass balance during weathering (Ma et al., 2010). Though smaller compared to WDC losses, relatively consistent dissolved losses of Th point to importance of organic complexation for what is generally a fairly insoluble element (Langmuir and Herman, 1980).

4.4. State factor influence on colloidal and solutional losses

Controls on the development of soils have been divided into five state factors: parent material, climate, topography, biota, and time (Jenny, 1941). Application of the dual-phase model in two contrasting

settings now provides perspective on the influence of state factors on colloidal and solutional mass redistribution in soils. Prior to the current study, the model was applied to a gently sloping (≤ 3°), granite-derived *catena*, developed under a semiarid climate in South Africa (Bern et al., 2015). There, maximum WDC mass losses relative to parent material ranged up to − 14%, and downslope Btn horizons had gained up to 56% WDC mass. Such values contrast with the ubiquitous and larger losses at SSHO (Table 4). The pattern is reversed for dissolved losses, which on the granitic catena were large and ranged − 27% to − 49%. By comparison, the maximum dissolved loss was only − 7% at SSHO.

Contrasts in all of the major soil forming factors likely account for the striking differences above. Granites, like the parent material of the catena, generally consist of coarse-grained minerals, and WDC losses from the catena may be less because chemical weathering is necessary to generate smaller secondary mineral particles before they can be mobilized as colloids. In contrast, the shale is composed of 45–68% illite and chlorite (Jin et al., 2010). Simple physical disaggregation is all that is required to release such clay minerals for subsequent dispersion and mobilization. Granites contain abundant feldspar and other igneous minerals susceptible to dissolution by chemical weathering. That fact, and the 150 kyr residence time of soils on the catena, help drive large mass losses via solution (Chadwick et al., 2013). Shales, by comparison, are composed of materials that have endured a previous cycle of continental weathering and transport by rivers to the ocean, largely eliminating minerals easily susceptible to dissolution weathering. That difference, and the shorter (7–40 kyr) residence times of mobile regolith (Ma et al., 2010; West et al., 2013) favor smaller solution losses at SSHO.

The gentle slope of the African catena causes surface and subsurface flows of water to be slow, allowing more time for mobilized WDCs to interact with and be retained by the soil matrix. The steep slope at SSHO (20°) causes faster flows of water, increasing the likelihood that WDCs, once mobilized, will exit the slope to the stream. Bioturbation is one factor whose influence on WDC mobilization seems unclear. The African catena is bioturbated in upslope areas by termites, but sparse woody vegetation suggests tree throw has little influence there (Levick et al., 2010). Bioturbation is thought to be somewhat limited in soils in the region of SSHO (Kaste et al., 2007), but there is evidence for some physical disturbance, including tree throws (Lin et al., 2006). Contrasting climates at the two sites likely influence dissolved and WDC mass losses in complex ways, but freezing temperatures at SSHO may be a key difference. Freeze-thaw cycles are an important process for soil mobilization at SSHO (West et al., 2014). However, freeze-thaw cycles also have been shown to markedly increase colloid mobilization from shale-derived soil in a laboratory setting (Mohanty et al., 2014), and may thus enhance WDC losses at SSHO.

From this preliminary assessment, it may be surmised that fine grained (≤ 1 μm) recalcitrant minerals in parent material, steeper slopes, wetter climates, and perhaps freeze-thaw cycles enhance WDC losses from soils. Of these, fine-grained, recalcitrant minerals may be particularly important, as illustrated by incipient shale weathering in bedrock fractures (Hasenmueller et al., 2017). Less recalcitrant mineralogy of parent material and longer regolith residence times likely drive greater solution losses. Application of the model in other settings will confirm or deny these patterns.

5. Conclusions

The loss of micron-sized mineral particles has previously been identified as an important soil-forming process at SSHO. Here the composition of WDCs isolated in the laboratory from SSHO soil was determined. WDCs were dominated by clay minerals, mostly inherited from the parent shale and presumably liberated by physical weathering, as opposed to secondary minerals generated by chemical weathering. Comparison of element concentrations in soil, WDCs, and shale parent material was used to infer the practical insolubility of five elements. Three of those elements (Al, Ga, Rb) partitioned preferentially into WDCs, and two (Zr, Hf) were preferentially excluded. Pairing these elements into tracer ratios, the dual-phase model was used to determine losses of overall mass and individual elements via WDCs and via solution.

WDCs dominated mass losses from soil, accounting for at least 90% of the total mass lost via WDCs and solution combined. Zirconium concentrations in the generally ≤ 1 μm WDCs were 97–158 ppm, although the nature of the Zr-bearing particles remains unknown. Mobilization via WDCs removed Zr from soil and the median Zr loss was 41% relative to parent material. After accounting for Zr lost via WDCs, the fraction of total denudation attributable to weathering, as opposed to erosion, was 0.6. The magnitude of this fraction in turn is primarily attributable to large mass losses via WDCs. Such patterns reflect the nature of the shale parent material, which contains abundant fine-grained minerals and is dominated by recalcitrant minerals previously subjected to continental weathering.

Losses of Zr had skewed previous determinations of elemental losses at SSHO via traditional mass balance using Zr as an index. Median total losses in different soil depth increments determined by the dual-phase model were greater for Al (36%), Fe (38%), Si (112%), Ti (73%), Ca (71%), Mg (31%), K (30%), and other elements, compared to traditional mass balance. The majority of Ca, Mg, and K losses occurred via WDCs, countering expectations that chemical weathering controls losses of base cations. Phosphorus, and to a lesser extent Ca, showed gains via solution at the soil surface that may be reflective of nutrient uplift or retention by biotic cycling.

These results for the steeply sloping, shale-derived soils of SSHO stand in stark contrast to moderate mass redistributions via WDCs observed for a gently sloping, granitic *catena*. However, in both settings, traditional mass balance determinations that assumed immobility for the index element Zr were systematically skewed by mobility of Zr in colloidal form. This bias is overcome by the dual-phase model, which yields additional insights by dividing weathering losses into dissolved and colloidal components. Although the dual-phase model includes its own assumptions, particularly the insolubility of selected tracer elements and adequate representation of WDC composition, these results suggest it is a valuable tool for improved understanding of the Earth's Critical Zone.

Supplementary data to this article can be found online at https://doi.org/10.1016/j.chemgeo.2017.11.040.

Acknowledgements

Financial support was provided by National Science Foundation (NSF) via a Seed Grant from EAR – 1331726 (S. Brantley) for the Susquehanna Shale Hills Critical Zone Observatory. Logistical support and data were provided by the NSF-supported Susquehanna Shale Hills Critical Zone Observatory. This research was conducted in Penn State's Stone Valley Forest, which is funded by the Penn State College of Agriculture Sciences, Department of Ecosystem Science and Management and managed by the staff of the Forestlands Management Office. Helpful discussions with Susan Brantley, Hyojin Kim, and Xin Gu improved this work. Comments on earlier drafts from Oliver Chadwick, Hyojin Kim, Marc Norman and five anonymous reviewers improved the paper. Heather Lowers and Bill Benzel of the USGS assisted with STEM and X-ray diffraction analysis, respectively. Any use of trade, firm, or product names is for descriptive purposes only and does not imply endorsement by the U.S. Government.

References

Barshad, I., 1955. Chemistry of soil development. In: Bear, F.E. (Ed.), Chemistry of the Soil. Reinhold Publishing Corp., New York, pp. 1–52.

Bau, M., 1996. Controls on the fractionation of isovalent trace elements in magmatic and aqueous systems: evidence from Y/Ho, Zr/Hf, and lanthanide tetrad effect. Contrib.

Mineral. Petrol. 123 (3), 323–333. http://dx.doi.org/10.1007/s004100050159.
Bénézeth, P., Diakonov, I.I., Pokrovsky, G.S., Dandurand, J.-L., Schott, J., Khodakovsky, I.L., 1997. Gallium speciation in aqueous solution. Experimental study and modelling: part 2. Solubility of α-GaOOH in acidic solutions from 150 to 250°C and hydrolysis constants of gallium (III) to 300°C. Geochim. Cosmochim. Acta 61 (7), 1345–1357. https://doi.org/10.1016/S0016-7037(97)00012-4.
Bern, C.R., Chadwick, O.A., 2010. Quantifying colloid mass redistribution in soils and other physical mass transfers. In: Birkle, P., Torres-Alvarado, I.S. (Eds.), Water Rock Interaction. CRC Press, Taylor & Francis Group, New York, pp. 765–768.
Bern, C.R., Chadwick, O.A., Hartshorn, A.S., Khomo, L.M., Chorover, J., 2011. A mass-balance model to separate and quantify colloidal and solute redistributions in soil. Chem. Geol. http://dx.doi.org/10.1016/j.chemgeo.2011.01.014.
Bern, C.R., Thompson, A., Chadwick, O.A., 2015. Quantification of colloidal and aqueous element transfer in soils: the dual-phase mass balance model. Geochim. Cosmochim. Acta 151, 1–18. http://dx.doi.org/10.1016/j.gca.2014.12.008.
Bern, C.R., Yesavage, T., Pribil, M.J., 2017. Iron isotope systematics of shale-derived soils as potentially influenced by small mineral particle loss. In: Proceedings of the 12th International Symposium on Applied Isotope Geochemistry (AIG-12): Copper Mountain, Colorado, (4 p.).
Brantley, S.L., White, A.F., 2009. Approaches to modeling weathered regolith. Reviews in Mineralogy and Geochemistry 70, 435–484. http://dx.doi.org/10.2138/rmg.2009.70.10.
Brimhall, G.H., Lewis, C.J., Ford, C., Bratt, J., Taylor, G., Warin, O., 1991. Quantitative geochemical approach to pedogenesis: importance of parent material reduction, volumetric expansion, and eolian influx in laterization. Geoderma 51, 51–91. http://dx.doi.org/10.1016/0016-7061(91)90066-3.
Chadwick, O.A., Roering, J.J., Heimsath, A.M., Levick, S.R., Asner, G.P., Khomo, L., 2013. Shaping post-orogenic landscapes by climate and chemical weathering. Geology 41, 1171–1174. http://dx.doi.org/10.1130/G34721.1.
Condie, K.C., 1991. Another look at rare earth elements in shales. Geochim. Cosmochim. Acta 55, 2527–2531. http://dx.doi.org/10.1016/0016-7037(91)90370-K.
Cornu, S., Quénard, L., Cousin, I., Samouëlian, A., 2014. Experimental approach of lessivage: quantification and mechanisms. Geoderma 213, 357–370. http://dx.doi.org/10.1016/j.geoderma.2013.08.012.
El-Farhan, Y.H., DeNovio, N.M., Herman, J.S., Hornberger, G.M., 2000. Mobilization and transport of soil particles during infiltration experiments in an agricultural field, Shenandoah Valley, Virginia. Environ. Sci. Technol. 34, 3555–3559.
Goldsmith, J.R., 1950. Gallium and germanium substitutions in synthetic feldspars. J. Geol. 58, 518–536. http://dx.doi.org/10.1086/625760.
Graham, C.B., Lin, H.S., 2011. Controls and frequency of preferential flow occurrence: a 175-event analysis. Vadose Zone J. 10, 816–831. http://dx.doi.org/10.2136/vzj2010.0119.
Hasenmueller, E., Gu, X., Weitzman, J., Adams, T., Stinchcomb, D.E., Drohan, P., Brantley, S., Kaye, J., 2017. Weathering of rock to regolith: the activity of deep roots in bedrock fractures. Geoderma 11–31. http://dx.doi.org/10.1016/j.geoderma.2017.03.020.
Herndon, E.M., Jin, L., Brantley, S.L., 2011. Soils reveal widespread manganese enrichment from industrial inputs. Environ. Sci. Technol. 45, 241–247. http://dx.doi.org/10.1021/es102001w.
Horbe, A.M.C., da Costa, M.L., 1999. Geochemical evolution of a lateritic Sn-Zr-Th-Nb-Y-REE-bearing ore body derived from apogranite: the case of Pitinga, Amazonas — Brazil. J. Geochem. Explor. 66, 339–351. http://dx.doi.org/10.1016/S0375-6742(99)00002-3.
Horstman, E.L., 1957. The distribution of lithium, rubidium, and caesium in igneous and sedimentary rocks. Geochim. Cosmochim. Acta 12, 1–28. http://dx.doi.org/10.1016/0016-7037(57)90014-5.
Jenny, H., 1941. The Factors of Soil Formation. McGraw Hill.
Jenny, H., Smith, G.D., 1935. Colloid chemical aspects of clay pan formation in soil profiles. Soil Sci. 39, 377–379.
Jin, L., Ravella, R., Ketchum, B., Bierman, P.R., Heaney, P., White, T., Brantley, S.L., 2010. Mineral weathering and elemental transport during hillslope evolution at the Susquehanna/Shale Hills Critical Zone Observatory. Geochim. Cosmochim. Acta 74, 3669–3691. http://dx.doi.org/10.1016/j.gca.2010.03.036.
Jin, L., Andrews, D.M., Holmes, G.H., Lin, H., Brantley, S.L., 2011. Opening the "black box": water chemistry reveals hydrological controls on weathering in the Susquehanna Shale Hills Critical Zone Observatory. Vadose Zone J. 110, 928–942. http://dx.doi.org/10.2136/vzj2010.0133.
Kaplan, D.I., Bertsch, P.M., Adriano, D.C., 1997. Mineralogical and physicochemical differences between mobile and nonmobile colloidal phases in reconstructed pedons. Soil Sci. Soc. Am. J. 61, 641–649.
Kaste, J.M., Heimsath, A.M., Bostick, B.C., 2007. Short-term soil mixing quantified with fallout radionuclides. Geology 35 (3), 243–246. http://dx.doi.org/10.1130/G23355A.1.
Kraepiel, A.M.L., Dere, A.L., Herndon, E.M., Brantley, S.L., 2015. Natural and anthropogenic processes contributing to metal enrichment in surface soils of central Pennsylvania. Biogeochemistry 123, 265–283. http://dx.doi.org/10.1007/s10533-015-0068-5.
Lægdsmand, M., Villhoth, K.G., Ullum, M., Jensen, K.H., 1999. Processes of colloid mobilization and transport in macroporous soil monoliths. Geoderma 93, 33–59.
Langmuir, D., Herman, J.S., 1980. The mobility of thorium in natural waters at low temperatures. Geochim. Cosmochim. Acta 44 (11), 1753–1766. http://dx.doi.org/10.1016/0016-7037(80)90226-4.
Levick, S.R., Asner, G.P., Chadwick, O.A., Khomo, L.M., Rogers, K.H., Hartshorn, A.S., Kennedy-Bowdoin, T., Knapp, D.E., 2010. Regional insight into savanna hydrogeomorphology from termite mounds. Nat. Commun. 1. http://dx.doi.org/10.1038/ncomms1066.
Lin, H., 2006. Temporal stability of soil moisture spatial pattern and subsurface preferential flow pathways in the Shale Hills catchment. Vadose Zone J. 5, 317–340. http://dx.doi.org/10.2136/vzj2005.0058.
Lin, H., Kogelmann, W., Walker, C., Bruns, M.A., 2006. Soil moisture patterns in a forested catchment: a hydropedological perspective. Geoderma 131, 345–368. http://dx.doi.org/10.1016/j.geoderma.2005.03.013.
Lynch, J.A., 1976. Effects of Antecedent Soil Moisture on Storm Hydrographs. PhD Dissertation. Pennsylvania State University, University Park, PA.
Ma, L., Chabaux, F., Pelt, E., Blaes, E., Jin, L., Brantley, S., 2010. Regolith production rates calculated with uranium-series isotopes at Susquehanna/Shale Hills Critical Zone Observatory. Earth Planet. Sci. Lett. 297, 211–225. http://dx.doi.org/10.1016/j.epsl.2010.06.022.
Ma, L., Jin, L., Brantley, S.L., 2011a. Geochemical behaviors of different element groups during shale weathering at the Susquehanna/Shale Hills Critical Zone Observatory. Appl. Geochem. 26, S89–S93 (doi: j.appgeochem.2011.03.038).
Ma, L., Jin, L., Brantley, S.L., 2011b. How mineralogy and slope aspect affect REE release and fractionation during shale weathering in the Susquehanna/Shale Hills Critical Zone Observatory. Chem. Geol. 290, 31–49. http://dx.doi.org/10.1016/j.chemgeo.2011.08.013.
Ma, L., Chabaux, F., Jin, L., West, N., Kirby, E., Brantley, S., 2013. Regolith production and transport at the Susquehanna Shale Hills critical zone observatory, part 1: insights from U-series isotopes. J. Geophys. Res. Earth Surf. 118, 722–740. http://dx.doi.org/10.1002/jgrf.20037.
Ma, L., Teng, F.-Z., Jin, L., Ke, S., Yang, W., H-O, Gu, Brantley, S.L., 2015. Magnesium isotope fractionation during shale weathering in the Shale Hills Critical Zone Observatory: accumulation of light Mg isotopes in soils by clay mineral transformation. Chem. Geol. 397, 37–50. http://dx.doi.org/10.1016/j.chemgeo.2015.01.010.
Markewich, H.W., Litwin, R.J., Wysocki, D.A., Pavich, M.J., 2015. Synthesis on quaternary aeolian research in the unglaciated eastern United States. Aeolian Res. 17, 139–191. http://dx.doi.org/10.1016/j.aeolia.2015.01.011.
Merrill, G.P., 1897. A Treatise on Rocks, Rock-Weathering and Soils. The McMillan Company, New York, New York.
Mills, T.J., Anderson, S.P., Bern, C.R., Aguirre, A., Derry, L.A., 2017. Colloid mobilization and seasonal variability in a semiarid headwater stream. J. Environ. Qual. 46, 88–95. http://dx.doi.org/10.2134/jeq2016.07.0268.
Mohanty, S.K., Saiers, J.E., Ryan, J.N., 2014. Colloid-facilitated mobilization of metals by freeze-thaw cycles. Environ. Sci. Technol. 48 (2), 977–984. http://dx.doi.org/10.1021/es403698u.
Noak, A.G., Grant, C.D., Chittleborough, D.J., 2000. Colloid movement through stable soils of low cation-exchange capacity. Environ. Sci. Technol. 34, 2490–2497. http://dx.doi.org/10.1021/es990708h.
Noireaux, J., Gaillardet, J., Sullivan, P.L., Brantley, S.L., 2014. Boron isotope fractionation in soils at Shale Hills CZO. Prog. Earth Planet. Sci. 10, 218–222. http://dx.doi.org/10.1016/j.proeps.2014.08.024.
Poppe, L.J., Paskavich, V.F., Hathaway, J.C., Blackwood, D.S., 2001. A laboratory manual for x-ray powder diffraction. U.S. Geol. Surv. Open File Rep. 01–041.
R Core Team, 2015. R: A language and environment for statistical computing. In: R Foundation for Statistical Computing, Vienna, Austria, (ISBN 3-900051-07-0, URL http://www.R-project.org).
Reimann, C., Filzmoser, P., Garrett, R.G., Dutter, R., 2008. Statistical Data Analysis Explained: Applied Environmental Statistics With R. John Wiley & Sons, Ltd., New York.
Riebe, C.S., Kirchner, J.W., Finkel, R.C., 2003. Long-term rates of chemical weathering and physical erosion from cosmogenic nuclides and geochemical mass balance. Geochim. Cosmochim. Acta 67, 4411–4427. http://dx.doi.org/10.1016/S0016-7037(03)00382-X.
Riebe, C.S., Kirchner, J.W., Finkel, R.C., 2004. Erosional and climatic effects on long-term chemical weathering rates in granitic landscapes spanning diverse climate regimes. Earth Planet. Sci. Lett. 224, 547–562. http://dx.doi.org/10.1016/j.epsl.2004.05.019.
Schindler, M., Hochella Jr., M.F., 2016. Nanomineralogy as a new dimension in understanding elusive geochemical processes in soils: the case of low-solubility-index elements. Geology 44 (7), 515–518. http://dx.doi.org/10.1130/G37774.1.
Seta, A.K., Karathanasis, A.D., 1997. Stability and transportability of water-dispersible soil colloids. Soil Sci. Soc. Am. J. 61, 604–611. http://dx.doi.org/10.2136/sssaj1997.03615995006100020033x.
Soil Survey Division Staff, 1993. Soil survey manual. In: Soil Conservation Service. 18 US Department of Agriculture Handbook.
Sudom, M.D., St. Arnaud, T.J., 1971. Use of quartz, zirconium and titanium as indices in pedological studies. Can. J. Soil Sci. 51, 385–396. https://doi.org/10.4141/cjss71-052.
Sullivan, P.L., Hynek, S.A., Gu, X., Singha, K., White, T., West, N., Kim, H., Clarke, B., Kirby, E., Duffy, C., Brantley, S.L., 2016a. Oxidative dissolution under the channel leads geomorphological evolution at the Shale Hills catchment. Am. J. Sci. 316, 981–1026. http://dx.doi.org/10.2475/10.2016.02.
Sullivan, P.L., et al., 2016b. CZ-tope at Susquehanna Shale Hills CZO: synthesizing multiple isotope proxies to elucidate critical zone processes across timescales in a temperate forested landscape. Chem. Geol. 445, 103–119. http://dx.doi.org/10.1016/j.chemgeo.2016.05.012.
Tejan-Kella, M.S., Fitzpatrick, R.W., Chittleborough, D.J., 1991. Scanning electron microscope study of zircons and rutiles from a podzol chronosequence at Cooloola, Queensland, Australia. Catena 18, 11–30. http://dx.doi.org/10.1016/0341-8162(91)90003-G.
Tole, M.P., 1985. The kinetics of dissolution of zircon ($ZrSiO_4$). Geochim. Cosmochim. Acta 49, 453–458. http://dx.doi.org/10.1016/0016-7037(85)90036-5.
Trostle, K.D., Runyon, J.R., Pohlmann, M.A., Redfield, S.E., Pelletier, J., McIntosh, J., Chorover, J., 2016. Colloids and organic matter complexation control trace metal

concentration-discharge relationships in Marshall Gulch stream waters. Water Resour. Res. 52. http://dx.doi.org/10.1002/2016WR019072.

West, N., Kirby, E., Bierman, P., Slingerland, R., Ma, L., Rood, D., Brantley, S., 2013. Regolith production and transport at the Susquehanna Shale Hills Critical Zone Observatory, part 2: insights from meteoric ^{10}Be. J. Geophys. Res. Earth Surf. 118, 1877–1896. http://dx.doi.org/10.1002/jgrf.20121.

West, N., Kirby, E., Bierman, P., Clarke, B.A., 2014. Aspect-dependent variations in regolith creep revealed by meteoric ^{10}Be. Geology 42 (6), 507–510. http://dx.doi.org/10.1130/G35357.1.

White, A.F., Blum, A.E., Schulz, M., Vivit, D.V., Stonestrom, D.A., Larsen, M., Murphy, S.F., Eberl, D., 1998. Chemical weathering in a tropical watershed, Luquillo Mountains, Puerto Rico: I. Long-term versus short-term weathering fluxes. Geochim. Cosmochim. Acta. http://dx.doi.org/10.1016/S0016-7037(97)00335-9.

Yesavage, T.F., M., S., Vervoort, J., R., M., Jin, L., Liermann, L.J., Brantley, S.L., 2012. Fe cycling in the Shale Hills Critical Zone Observatory, Pennsylvania: an analysis of biogeochemical weathering and Fe isotope fractionation. Geochim. Cosmochim. Acta 99, 18–38. http://dx.doi.org/10.1016/j.gca.2012.09.029.